Cenozoic Landscape Evolution of the Grand Canyon Region, Arizona

by

Copyright 2007
John P. Lee

B.S., Texas A&M University, 2005

Submitted to the Department of Geology and the

Faculty of the Graduate School of the University of

Kansas in partial fulfillment of the requirements for the

degree of Master of Science

_____

Dr. Daniel F. Stockli (Chairman)

_____

Dr. Michael H. Taylor

_____

Dr. J.F. Devlin

Date Defended: _____

The Thesis Committee for John Lee certifies at this is the approved version of the following thesis:

Cenozoic Landscape Evolution of the Grand Canyon Region, Arizona

Committee:

_____
Chairperson

Date approved:_____

Abstract

Cenozoic Landscape Evolution of the Grand Canyon Region, Arizona

By

John Lee

Dept. of Geology, December 2007

University of Kansas

The landscape evolution of the southwestern Colorado Plateau has eluded accurate description due to the scarcity of a Cenozoic rock record. However, advances in low-temperature thermochronology have shown the ability to quantitatively assess erosion patterns by recording the thermal history of rocks in the subsurface. This study utilizes apatite (U-Th)/He and fission track analysis of a several newly collected datasets to constrain the unroofing of the Grand Canyon region. Assessment of topographic evolution of the Kaibab Uplift is accomplished through 3-dimensional thermokinetic modeling of real and synthetic erosion and landscape evolution scenarios. Results illustrate the sensitivity of low-temperature thermochronometric ages to topography and also provide constraints on the erosion history atop the Kaibab Uplift. Investigation of a lateral transect outlines the regional unroofing patterns throughout the Grand Canyon region and support conclusions from assessment of additional vertical transects and borehole data.

Acknowledgements

Funding for this project was provided by the University of Kansas Dept. of Geology and NSF grants EAR-0408787 and EAR-0414817.

Thanks go Eugene Szymanski, Alec Waggoner, Kwan Ye Chen, Steve Sloan, and Randy Ackerman for hauling hundreds of pounds of rocks from the bottom of the Grand Canyon. I would like to thank Chris Hager, T.J. Dewane, Stephanie Brichau, for endless training and support in the lab. Thanks to all the faculty and staff at the KU Department of Geology and in particular my committee members Mike Taylor and Rick Devlin. Finally, a thanks to my coauthors: Todd Ehlers, Joel Pederson, and Shari Kelley and especially Daniel Stockli for input, patience, and the wonderful opportunities he has made possible.

TABLE OF CONTENTS

Introduction

This project was initiated by Daniel Stockli, as part of a multidisciplinary, NSF funded investigation of uplift and unroofing patterns across the Colorado Plateau. The following two chapters outline research towards investigating the landscape evolution and erosional unroofing of the southwestern portion of the Colorado Plateau in the region of the Grand Canyon, Arizona. Both studies utilize low-temperature thermochronology to quantitatively asses the thermal history recorded in rock as a result of erosion and topographic evolution.

Chapter 1 attempts to constrain the Cenozoic topographic development of the Kaibab Uplift through inspection of a pair of apatite (U-Th)/He vertical transects. Vertical transect samples were collected from the North and South Kaibab trails in the eastern Grand Canyon by John Lee, Alec Waggoner, and Eugene Symanzski in October, 2005. Mineral separation and sample analysis was done by John Lee at the University of Kansas. Investigation utilizes thermokinetic modeling of synthetically produced 3-dimensional landscape evolution and erosion scenarios to quantify the effects of canyon-like topographies on (U-Th)/He age distributions. A variety of parameters, including canyon presence, size, geometry, erosion rates, and topographic change are explored. Diagnostic age patterns are identified to aid in the assessment of paleo-topographic signatures in age distributions. These results are then applied to the continued modeling of the observed (U-Th)/He age dataset to constrain the viable landscape evolution history of the region. Modeling efforts establish best fit erosion scenarios where samples cool in either the presence or the absence of a paleocanyon. The results illustrate the profound

impact consideration of paleotopography can have on the interpretation of a low-temperature dataset.

Chapter 2 presents apatite (U-Th)/He and Fission Track data from two additional vertical transects, four boreholes (courtesy of USGS core research facility, Denver, CO), and a lateral transect spanning from Lees Ferry, AZ to the western Grand Canyon. The aim of this study is to establish a regional unroofing pattern, specifically in the lateral sense, to assess landscape and drainage evolution in response to known tectonic events. Inverse modeling is utilized to establish representative close temperatures and ultimately allow accurate calculation of the overburden thickness at the time of a sample's age closure. The results are presented in the form of unroofing profiles that outline the lateral patterns and variations in erosion through the Grand Canyon region. Lateral unroofing patterns are based on overburden calculations from the lateral transect, initially collected and analyzed for apatite fission track ages by and published by Shari Kelley and reanalyzed for (U-Th)/He ages by John Lee at the University of Kansas. Borehole samples and the additional transects were also analyzed by John Lee and support the conclusions drawn from quantitative treatment of the lateral transect. Both studies serve to provide constraints on erosional patterns and landscape evolution of the Grand Canyon throughout the Cenozoic.

CHAPTER 1: Quantifying the Evolution of Grand Canyon Topography with Thermochronology and Numerical Modeling

Chapter Summary

This study revisits a long-standing debate regarding the Cenozoic erosion history of the proto-Colorado River and Grand Canyon, Arizona. How and when the upper Colorado River established its course across Laramide-age uplifts has been difficult to ascertain due to a lack of early Cenozoic drainage system indicators. End-member scenarios predict the presence (i.e. antecedence) or lack (i.e. superposition) of a Laramide-age paleocanyon. We present new low-temperature thermochronometer data and 3D thermo-kinematic erosion and age prediction modeling to quantify the topographic history of the eastern Grand Canyon. Apatite (U-Th)/He (AHe) data were collected from two vertical transects along the North and South Kaibab trails. The numerical modeling predicts 3D and transient thermal field and thermochronometer cooling ages for sample locations. Model inputs include user defined erosion rates and histories, thermophysical rock properties, and basal crust and surface temperatures. Predicted and observed cooling ages were compared to test between the end-member models for canyon evolution. AHe ages from the two vertical transects range between 60 and 35 Ma and provide new constraints on the exhumation history of Mesozoic overburden from the Kaibab Uplift during the middle Cenozoic. Over 100 model simulations were used to explore a range of input parameters for the two end-member topographic evolution scenarios and the results are as follows: (1) Laramide-age canyon models produce predicted ages within the 2σ age uncertainty of observed ages and indicate an erosion rate of ~300 m/myr that abruptly changes to 30 m/myr at 60Ma.

Further changes in erosion rates throughout the Neogene are unnecessary to provide the best fit. (2) Results for middle Cenozoic erosion without the presence of significant paleo-relief produces predicted ages that fall within 1σ of observed ages and indicates a late Cretaceous to late Eocene erosion rate of 70 m/myr, followed by an erosional hiatus during the late Oligocene to middle Miocene. Penetration of the Kaibab surface by ~30Ma is required to fit lower elevation samples and indicates a change to a more incisive erosional style. Both best-fit results suggest the presence of a middle Cenozoic canyon on the Kaibab Uplift spatially coincident with the modern Grand Canyon.

1. Introduction

The long-term erosional evolution of landscapes and the formation of topographic relief is the product of the complex interplay of tectonics, climate, and geological boundary conditions. Theoretical and applied aspects of the linkage between these factors, and the importance of their effects on geodynamic processes have attracted considerable debate over the past decade (Schlunegger and Willett, 1999; Whipple et al., 1999; Reiners et al., 2003; Whipple and Meade, 2004). The timing and rates of processes in response to changes in climatic or tectonic forcing remain critical to elucidate linkages and distinguish processes. The tectonic and topographic development of orogenic plateaus has been at the center of this debate, with canyon incision along plateau margins being used to shed light on the timing and rates of erosion and surface uplift (Clark et al., 2005). The timing and rate of incision is commonly difficult to constrain, however, since the geological record is removed and can only occasionally be tracked through punctuated time markers (Stock et al., 2004; Haeuselmann et al., 2007). The application

of low-temperature thermochronology for assessing long-term landscape evolution has become a commonly used approach to constrain the magnitude and timing of erosional exhumation (e.g. House et al., 1997; Ehlers and Chapman, 1999; Braun, 2002; Brown et al., 2002; Braun, 2005; Clark et al., 2005; Shuster et al., 2005; Ehlers et al., 2006). It has been demonstrated theoretically and empirically that relief generation, such as river incision, leads to systematic deflection of isotherms in the shallow crust (<5 km) due to topographic cooling, with the geometry of deflected isotherms being a function of the topographic amplitude and wavelength (Stuewe et al., 1994; Mancktelow and Grasemann, 1997; Braun, 2002; Ehlers and Farley, 2003). Therefore low-temperature thermochronology can be used to reconstruct perturbed closure isotherms and hence provide constraints on the timing and magnitude of topographic relief generation and relief change through time (Braun, 2002). Several studies have attempted to extract information on long-term landscape evolution and eroded paleo-landscape from low-temperature thermochronometric datasets (e.g. House et al., 1997; Armstrong et al., 2003; Braun, 2005; Shuster et al., 2005).

In this study, we combine new low-temperature thermochronometric data with 3-D thermokinematic modeling to decipher and quantify the long-term landscape evolution of the eastern Grand Canyon, Arizona. A detailed understanding of the Cenozoic landscape and drainage evolution in the Grand Canyon region is limited by the lack of Cenozoic/Mesozoic rock record. However, laterally homogeneous thermophysical properties, high amplitude (>1.5 km) and wavelength (>10 km) relief, and little post-Laramide structural deformation make the eastern Grand Canyon region an excellent case study to explore the theoretical effects of canyon cutting on the upper-crustal thermal

structure and low-temperature thermochonometric data and to elucidate the canyon's Cenozoic landscape evolution by low-temperature thermochronometry. Numerical modeling of real and synthetic landscape evolution scenarios allows exploration of the effects of different canyon geometries and timing of canyon cutting on thermochronometric age distributions. These new analytical and numerical modeling results offer the exciting chance to revisit and answer some of the long-standing questions regarding the timing of incision of the Colorado River and erosion of the Colorado Plateau in the eastern Grand Canyon region. Furthermore, this case study also offers new insights into modeling techniques for assessing the long-term incision history of large canyons.

2. Background and Approach

2.1 Geologic Setting

The Colorado Plateau of the western United States is characterized by an average elevation of ~2 km and has experienced significant amounts of surface and rock uplift and erosional exhumation since the late Cretaceous, despite the relative lack of internal structural deformation (Pederson et al., 2002b; Roy et al., 2004a). Many studies of the region have investigated how and when the plateau obtained its high elevation and the link to processes involved in creating the considerable volumes of incision. Erosional sculpting and river incision has created a spectacular landscape that has lead to the creation of some of world's most visited national parks. Undoubtedly, the most notable of these erosional landforms is the Grand Canyon of the Colorado River, with a maximum vertical relief of ~1.6 km. The geology of the Grand Canyon is dominated by a little

deformed Paleozoic stack of siliciclastic and carbonate sediments deposited on the long-lived western North America passive continental margin (Beus and Morales, 2003a). These Cambrian to Permian sediments overlie Proterozoic sediments and metamorphic basement, exposed at the modern river level of the Colorado River in the eastern Grand Canyon (Karlstrom et al., 2003).

Geomorphologically, the Colorado River flows against a regional, gently east-dipping topographic and structural grain of the southwestern margin of the Colorado Plateau in the eastern Grand Canyon. The river, also, cuts across Laramide-aged basement uplifts such as the Kaibab Uplift (Fig. 1). The history of the Colorado River and the establishment of its unlikely course have been the topic of considerable debate, largely due to the relatively sparse Mesozoic and Cenozoic sedimentary rock record on the southwestern portion of the Colorado Plateau. An early-Cenozoic, east-draining fluvial system is recorded in scattered outcrops of gravels on the southwestern boundary of the Colorado Plateau that were shed from denuding source terrains to the south and west of the modern edge of the Colorado Plateau (Young, 1979; Bilodeau, 1986; Burchfiel et al., 1992; Young, 2000). Due to an almost complete lack of middle Cenozoic rock record, little is known about the evolution of the drainage system until the Pliocene arrival of an integrated, west-flowing Colorado River into the adjacent Basin and Range. The Grand Wash Trough, which currently demarks the normal fault-bounded border of the southwestern Colorado Plateau and modern exit point of the Colorado River from the Colorado Plateau, was established by ~13 Ma (Faulds et al., 2000a) and contains the late-Miocene sedimentary record of the transition from an east- to west-draining, through-flowing Colorado River at ~5-6 Ma (Castor and Faulds, 2000; Faulds et al.,

2000a; Faulds et al., 2000b; Pederson, 2000). Unfortunately, exact timing of this drainage reversal remains poorly constrained, as is the timing and spatial style of erosional removal of Mesozoic strata that once covered the Grand Canyon region. One of the fundamental questions this study is trying to answer is the question of the timing and temporal and spatial variation of the magnitude of canyon cutting in the eastern Grand Canyon. The following section summarizes possible end-member landscape evolution scenarios for the eastern Grand Canyon.

2.2 End-member Erosion Scenarios

For the purposes of this study, landscape evolution scenarios that explain the modern course of the Colorado River in the region of the eastern Grand Canyon can be divided into two end-member scenarios (see Fig. 2). This study explores a set of geometric and temporal parameters that characterize each of the end-member scenarios as well as a spectrum of intermediate scenarios. The early canyon scenario predicts the presence of an antecedent, incising, east-flowing pre-Laramide-aged river system. This scenario results in early entrenchment of the east-flowing Colorado River during the growth of the Kaibab Monocline and results in a paleo-canyon in the Laramide. In this case, samples cool in a setting of high relief. In contrast, the late canyon-cutting scenario predicts Laramide planation and/or covering of topographic highs, creating a broad low-relief erosion surface. After this time, the establishment of a late, superimposed, and integrated river system could then incise through the remaining Mesozoic overburden and the underlying Kaibab Uplift at some time after the cooling of the Grand Canyon samples. In this case, samples cool in a setting of low relief and generation of significant

paleotopography occurs sometime after the closure of the lowest vertical transect samples at ~35 Ma. These two scenarios results in very different cooling histories for rocks below the incising canyon and thus provide thermochronometrically testable hypotheses. While the presence of Laramide-aged paleotopography would make the antecedent river scenario viable, the absence of such paleotopography would verify that a superimposed (i.e. late-canyon erosion scenario) river system is the likely explanation for the course of the Colorado River through modern topographic highs.

2.3 Approach and Methodology

2.3.1 Isotherm Deflection

The effects of topographic cooling in areas with high-amplitude, long-wavelength topography has been shown to significantly perturb the geometries of upper crustal isotherms (< 5 km). This deflection of isotherms from horizontal is dampened with depth, but can significantly affect the interpretation of thermal histories derived from low-temperature thermochronometric data (Stuewe et al., 1994; Mancktelow and Grasemann, 1997; Braun, 2005; Ehlers, 2005). Although this effect ads an additional complication when quantitatively constraining cooling histories in orogenic systems, recent studies have very elegantly inverted topographic and transient thermal effects to reconstruct paleotopography and the timing of relief amplification or reduction using numerical modeling (House et al., 1997; Ehlers et al., 2006). The geometry and/or spacing of isotherms is influenced by several parameters, such as topographic wavelength and amplitude (Stuewe et al., 1994; Mancktelow and Grasemann, 1997), the timing of topographic relief change (Braun, 2002), changes in erosion rates (Ehlers, 2005),

spatially variable surface temperatures (e.g. lapse rates), groundwater flow (Whipp and Ehlers, 2007), as well as laterally heterogeneous thermophysical properties of the rocks underlying the topography.

In the absence of any transient effects and thermophysical heterogeneities, the magnitude of isothermal perturbation is controlled by the first-order shape of the topography and is directly proportional to topographic wavelength and amplitude. The critical wavelength (ω_c), as described by Braun (2005), describes a minimum wavelength at which topographic features begin to significantly deflect the geometry of closure isotherms and therefore, the thermochronometric age for a given geothermal gradient (G_o) and closure temperature (T_c). This relationship can be expressed as $\omega_c=T_c/G_o$. In the case of the Grand Canyon, topographically induced isotherm perturbation affecting apatite (U-Th)/He ages should occur at wavelengths > 2 km (assuming a G_o of 25ºC/km and a T_c of ~50ºC), while near-complete isothermal/topographic tracking occurs at topographic wavelengths of >20 km. In the case of the eastern Grand Canyon, modern topography encompasses this range of topographic wavelengths and deflection of modern isotherms due to topography should occur and needs to be anticipated. It is worth stating, however, that the observed thermochronometric age distribution is not a function of the modern topography, but rather the cumulative temporal and spatial effects of erosion and relief generation (i.e., incision) during landscape evolution.

2.3.2 Numerical Modeling

Three dimensional quantification and meaningful interpretation of paleotopographic effects often requires the use of numerical modeling software to solve the thermal diffusion equation. This study utilizes a modified version of Pecube, a

numerical modeling software package that solves the 3-D advection/diffusion equation to calculate thermal histories for prescribed erosion rates and landscape evolutions at user defined sample locations (Braun, 2003). Primary model parameters include, (1) thermophysical parameters characterizing the modeled crustal block, such as thermal diffusivity, radiogenic heat production, base temperature, model depth, etc., (2) digital elevations model (DEM) data, real or synthetic, that describe the surface topography at various time steps (used to define topographic evolution), and (3) user prescribed erosion rates. Pecube assumes a medium of homogeneous thermophysical properties.

Pecube 3-D numerical modeling tracks the thermal history of the entire model and thus for specified samples locations allows calculating ages of different thermochronometers with specified diffusion/annealing kinetics. The comparison of observed and modeled ages from a suite of samples for different erosion histories, such as the late and early canyon incision end-member scenarios, should allow us to (1) quantify the effects of Grand Canyon scale topography and identify indicators diagnostic for the presence of paleotopography and (2) frame the best fit erosion scenario results against observed (U-Th)/He and fission track data and known geologic constraints to determine viable landscape evolution histories for the Grand Canyon region.

2.3.3 Apatite (U-Th)/He Thermochronology

Apatite (U-Th)/He (AHe) dating as a low-temperature thermochronometer has been applied to a variety of geologic studies. The (U-Th)/He dating technique is based on the decay of ^{235}U, ^{238}U, ^{232}Th, and ^{147}Sm by alpha (^{4}He nucleus) emission. ^{4}He is completely expelled from apatite at temperatures above ~80°C and almost totally retained

below ~40°C (termed the Partial Retention Zone or PRZ) (Stockli et al., 2000). Raw ages are determined from the concentrations of radioactive parent (^{235}U, ^{238}U, ^{232}Th, and ^{147}Sm) and daughter (^{4}He) isotopes. The decay energy, up to ~8 MeV, is taken up in the form of α-recoil of the parent nucleus and energetic emission of the α particle (Farley et al., 1996). Alpha particles are emitted with high kinetic energy and travel significant distances before coming to rest, leading to potential α loss during decay. Thus, measured (U-Th)/He ages are reduced by this ejection effect; an ejection effect that is commonly and viably corrected for using a statistical approach taking into account mineral density and crystal geometry (Farley et al., 1996).

Several physical parameters have been shown to affect He diffusivity in apatite. Grain size has been shown to positively correlate with (U-Th-Sm)/He ages (Farley, 2000; Reiners and Farley, 2001) such that ages from smaller grains represent closure at lower temperatures than larger grains. Shuster and others (2006) demonstrated that He retentivity correlates with total radiation damage. This relationship is readily observable in the correlation of (U-Th)/He ages with the effective U concentration (i.e., U + 0.235Th) and can dramatically affect samples that experienced protracted cooling or moderate reheating during burial (Flowers et al., 2007). In this study, Pecube generated (U-Th)/He ages are calculated using Farley (2000) diffusion kinetic parameters.

Because the AHe and AFT thermochronometers record the migration of a thermal field at a single point in time, 2- and 3-D sample sets are often collected to inspect the migration of a thermal field through time (see Stockli, 2005). Erosion rates are commonly assessed by plotting elevation against age for samples collected from near-vertical transects. A regressed line connecting data points represents the cooling rate. In

areas of horizontal and static thermal fields, this cooling rate is often a direct reflection of the unroofing rate. However, deviations and/or changes in thermal structure (e.g. the presence of topography), as well as changes in erosion rates, can both lead to a loss of linearity in an age/elevation relationship.

3. Synthetic Canyon Modeling

3.1 The Synthetic Canyon Approach

Departures from linear age/elevation relationships, as a result of topography, can be due to both large-scale (Fig. 3) and small-scale (Fig. 4) topography (also see section 3.4). Because the magnitude of isotherm deflection is a function of wavelength, samples collected on differing scales of topographic features can express differing age/elevation relationships. To eliminate this interference, this study uses two, highly smoothed, synthetic, topographic models with geometries approximating an idealized eastern Grand Canyon. These topographic models allow the assessment of age data deviation as a direct result of the large scale topography, independent of small-scale topographic effects that would be applicable to a wide range of canyon-like topographic and erosion scenarios. By utilizing this method, it is possible to quantitatively assess the patterns and changes we might expect to see in the eastern Grand Canyon thermochronometric age data as a result of canyon geometry, relief change, and changes in erosion rate. It should be noted, however, that synthetic canyon results are not meant to place quantitative constraints on the Grand Canyon's unroofing history. The use of synthetic canyon modeling is only intended to asses the magnitude and pattern of effects we should expect to see as a result of paleotopography on the scale of the Grand Canyon. Later sections of this study will

directly investigate variable erosion scenarios within the framework of existing geologic constraints in order to constrain an erosion history specifically for the Grand Canyon.

For this study, topographic models were created to represent an environment that is representative of the eastern Grand Canyon area with smoothed small-scale topography (Fig. 5). Because of the variable asymmetry commonly observed in Grand Canyon cross sections, two models were created. The first model, referred to as the symmetric-canyon, is a symmetric and simplistic representation of the central Grand Canyon (e.g. the Tuweap region) and is used to assess paleotopograhic effects in the most simplistic erosion scenarios. The second model, referred to as the asymmetric-canyon, is a more realistic representation of the eastern Grand Canyon cross-section across the Kaibab uplift. Thermophysical properties used in the synthetic canyon simulations are representative for the Grand Canyon region (Table 1). See appendix A for discussion on the derivation of these values.

Using Pecube, a series of models were generated using both canyon models as well as a zero-relief (peneplain) model. The different model runs and scenarios were used to explore the following parameters and conditions: (1) erosion rate (both steady-steady state and variable), (2) the presence or lack of topography, (3) the timing of onset and the rate of incision, (4) canyon geometry (v-canyon or asymmetric-canyon), and (5) the effects of geometry changes through time.

3.2 Synthetic Canyon Modeling Results

3.2.1 Late Canyon Erosion Scenarios

Late Canyon erosion scenarios consisted of wholesale erosion of a flat-lying, zero-relief surface (planation) followed by a cessation of regional erosion and localized incision of a canyon (see Fig. 2A). Pseudo-vertical transects are created by extracting predicted ages from a linear array of surface nodes across the canyon. Model runs using planation erosion histories and static erosion rates (Figs 6A and 6B) exhibited three characteristic attributes, (1) highly linear age/elevation relationships in scenarios involving static erosion rates, with changes in erosion rates reflected by changes in slope of the age/elevation relationship. (2) Apparent erosion rates (Ea) (i.e., slope of age/elevation data points) matched 'true' or input erosion rates (Et) to within 15% difference. The small disagreement between Ea and Et can be attributed to the non-steady-state nature of isotherms in eroding environments (Ehlers, 2005) and the continued diffusion (and age skewing) due to sample depth. (3) Spatially different age/elevation relationships are invariant. Because isotherm geometry is homogenous laterally, ages are independent of lateral position or canyon geometry.

3.2.2 Early Canyon Erosion Scenarios

Early canyon erosion scenario models are characterized by an initial topography exhibiting a canyon and subsequent progressive erosion preserving the shape of the original topography (see Fig. 2B). Canyons of both symmetric and asymmetric type were used to asses the influence of isotherm perturbation on age data for canyons of varying geometry and size. Characteristic attributes of these paleo-canyon model runs are illustrated in figure 6 and are summarized in the following sections that also describe the important effects of these scenarios on the thermochronometric data interpretation.

(1) Calculating erosion rates: Erosion rates are often calculated from thermochronometric vertical transect data utilizing the age versus elevation relationship. The slope of a line fitted to these data points yield an apparent erosion rate. Previous studies (Stuewe et al., 1994; Mancktelow and Grasemann, 1997; Braun, 2002) have demonstrated that paleo-topography can systematically increase or decrease apparent erosion rates. In this study, erosion and landscape evolution scenarios were modeled to quantify the effects of varying canyon size and geometry for a broad range of erosion rates and differing canyon geometries. Model derived apparent erosion rates (Ea) commonly overestimate the prescribed true erosion rates (Et) by a factor of 2-3 (Fig. 7). This overestimation was found to be proportional to canyon width (i.e. topographic wavelength). Overestimation of the erosion rate was also inversely proportional to erosion rates below ~300 m/my and proportional to erosion rates greater than ~300 m/my. This change in proportionality is due to the loss of steady state isotherm structure in rapidly eroding environments where increased geothermal gradients due to rapid erosion leads to forced (i.e. non-steady state) isotherm deflection around the canyon.

(2) Canyon geometry: Deviations in age/elevation relationship from linearity, as a result of paleo-topography is directly related to the magnitude of 'decoupling' of the topographic surface and the closure isotherm at depth during the time of age closure for a sample. Because isotherm deflection leads to laterally variable isotherm depth, samples of equal elevation can correspond to different ages, resulting in a variant age/elevations relationship. This age variance is most easily identified by a deviation from linearity in an age/elevation plot. However, it should be noted that after applying a standard 6% 2-σ uncertainty to the modeled ages, such patterns are often largely concealed.

(3) Recent geometry change: Excavation from a symmetric canyon to an asymmetric canyon after the samples have passed through the PRZ results in contrasting age/elevation relationships for each canyon wall. Because of the presence of deflected isotherms, samples lying at increasing distances from the canyon axis are exhumed through isotherms with decreasing deflection. For this reason, samples now exposed on the exhumed surface undergo cooling histories that more closely resemble the cooling history of the surrounding plateau, outside of the influence of the canyon. The shallower age/elevation relationship of the exhumed surface samples more closely matches the true erosion rate, and the younger ages represent the ages that would occur in a setting with decreased isotherm deflection. The magnitude of separation between age/elevation relationships of the unchanged and excavated surfaces is therefore, directly related to the degree of isotherm deflection and the amount of excavation.

3.3 Small Scale Topographic Effects

In the presence of isotherm deflection as a result of the presence of significant paleotopography, small scale (<2 km) topographic features can help in revealing isotherm deflection and its effects on age distributions (see Fig. 4). Due to the loss of age/elevation invariance, samples collected from local topographic highs (e.g. ridges) and lows (e.g., secondary drainages) correspond to older and younger ages, respectively. The result of this short wavelength topographic effect is an increased amount of 'noise' or age-scatter along a vertical transect. The magnitude of this effect is higher on features with a high amplitude-to-wavelength ratio, whose wavelength is small enough to incur small perturbation of the underlying closure isotherm. This effect is largely the result of

the dampened effects of topography with depth (also see Braun, 2002). Differing degrees of isotherm deflection from topographic features of differing scale and wavelength leads to variations in the age/elevation relationships and a resulting departure from linearity. In this sense, contrasting age/elevation relationships from short- and large-wavelength features might indicate cooling through deflected isotherms.

3.4 Summary of Paleotopographic Effects on Age Distributions

Results of >100 modeled scenarios have allowed the characterization of the thermal structure underlying a synthetic canyon for a wide range of erosion and geometric variations. These results suggest that it is possible to investigate the presence or absence of paleotopography similar to that of the Grand Canyon. Indicators applicable to vertical transect datasets include the following: (1) Samples that are cooled in environments with little isotherm perturbation (e.g., environments without significant paleotopography) and constant erosion rates should exhibit linear age/elevation relationships. In this sense, samples of a certain elevation roughly correspond to certain ages as defined by the erosion/cooling history, regardless of location inside or outside the topographic feature of interest. To best test this indicator, sample collection should also lie outside of the main topographic feature and include multiple samples at equivalent elevations within a coherent structural block. (2) Apparent erosion rates closely match true erosion rates for scenarios with little isotherm perturbation. While small (< ~15%) differences in calculated and observed erosion rates can be due to a loss of steady state thermal fields commonly associated with the onset or cessation of erosion, significant changes in erosion rates are directly represented by changes in the Et. (3) Warping of isotherms due

to large scale topographic features often results in the shifting and/or rotation of age/elevation data trends that can lead to a significant under- or overestimation of true erosion rates. It should be noted that scenarios with isotherm deflection can produce age/elevation datasets that mimic age/elevation trends of scenarios without isotherm deflection by simply prescribing a different erosion rate. However, if the true erosion rate is known from other geologic evidence, mismatch of Et and Ea may help quantify the magnitude and geometry of paleotopography. (4) In scenarios with significant isotherm deflection, small scale topographic features can result in scattered age data where small scale topographic highs correspond to older ages and small scale topographic lows correspond to younger ages. For this reason, it may be useful to collect vertical transect data from as wide a variety of topographic features as possible. (5) Topographic geometry changes after the age closure, as a result of asymmetric canyon excavation, can lead to easily observable age deviations that represent the attenuated effects of isothermal deflection at increasing distances from the canyon.

4. Grand Canyon (U-Th)/He Data and Modeling

4.1 The Kaibab Transects

A total of 29 new samples were collected in the eastern Grand Canyon from both the North and South Kaibab trails, of which 21 samples yielded enough quality apatite to produce (U-Th)/He ages (Fig. 1, Table 2). The North Kaibab transect yielded 7 ages over an elevation span of 1.63 km. The South Kaibab transect produced 14 ages (including 3 outliers) and spanned 1.40 km vertically.

The contrasting topographic geometries of the two transects are of particular importance (Fig. 9). The South Kaibab transect was collected along an inter-drainage ridge extending from the South Rim to the Colorado River; a short-wavelength topographic high. In contrast, the North Kaibab transect was collected along the Bright Angel drainage, a short-wavelength topographic low. In addition, the shorter South Kaibab transect has a highly linear age profile, while the longer North Kaibab transect exhibits a concave up profile

4.1.1 Apatite (U-Th)/He Age Data

Apatite (U-Th)/He ages, excluding three outliers, range from 59.8 Ma on the North Rim and 51.8 Ma on the South Rim, to 36.8 Ma at the Colorado River (Fig. 10). Age uncertainties are standard errors ($\sigma\sqrt{n}$) for samples with $\geq$4 analysis and one sigma errors (σ) for samples with <4 analysis. Samples were collected from a variety of lithologies, including quartz arenites, micritic limestones, biotite schists, and yield ages significantly younger than depositional ages. This indicates that all samples have likely been completely thermally reset which is in agreement with previous thermochronometric work in the area (Dumitru et al., 1994; Kelley et al., 2000; Flowers et al., 2007).

The North and South Kaibab transects exhibit very similar age/elevation patterns. Apatite (U-Th)/He ages from both transects yield highly linear age/elevation relationships with apparent erosion rates of 83 m/my (South Kaibab) and 81m/my (North Kaibab). In addition, the absolute ages of both transects overlap within error despite the contrasting transect profiles.

Average effective uranium concentrations ([eU]) range from 3 to 71 ppm. Single grain apatite analysis with <2 ppm were discarded due to ICP-MS sensitivity limits and large resulting analytical uncertainties. Because of the effects of alpha radiation damage on diffusion kinetics of very high [eU] grains, this study also excluded analysis whose [eU] exceeded 200ppm or if the analysis was greater than twice the typical [eU] for the sample from mean age calculations (see table 3 for all age analyses). This narrowing of [eU] allows for better characterization of analysis averaged samples when using diffusion parameters that incorporate the effects of alpha radiation damage on diffusion kinetics and enhanced retentivity (Shuster et al., 2006). Results incorporating analysis of all [eU] are currently in progress.

4.1.2 Apatite Fission Track Data

Previously published apatite fission track (AFT) data exists from the South Kaibab trail and has been incorporated into this study (Dumitru et al., 1994). These fission track ages range in age 143 ± 15 Ma near the canyon rim to 61 ± 4 Ma at the Colorado River. Samples collected along the South Kaibab record a downward trend of increased annealing due to burial by Mesozoic sedimentary cover and place constraints on the maximum thickness of overburden across the Kaibab Uplift. The four lowest samples in the study have highly reproducible ages of 61-66 Ma. Average tracks lengths of 12.0-12.6 μm indicate track shortening during protracted cooling and residence at elevated temperatures (~45-75°C). Since Pecube does not account for the effect of age reduction due to track shortening, this study utilizes Dumitru and others (1994) corrected ages of 75 ± 6 Ma for the initial cooling.

4.2 Grand Canyon Modeling Results

Numerical modeling results using simplified canyon geometries show that effects of paleotopography, on the scale (i.e., wavelength and amplitude) of the modern Grand Canyon, are likely to significantly distort apatite (U-Th)/He closure isotherms and thus affect the spatial age distribution. Synthetic canyon modeling results also show that it is possible to produce similar age/elevation distributions from vertical sample arrays for different erosion histories due to the effects of paleotopography. The spectrum of possible erosion histories for the eastern Grand Canyon and the Kaibab uplift is investigated by exploring erosional landscape evolution models with either the presence of a large paleo-canyon (i.e. early canyon) or the absence of significant paleotopography. The process for producing a best-fit erosion history for each of the end member scenarios involves a two-step approach that is repeated in an iterative fashion. In a first step, parameters controlling the slope and shape of age/elevation data points are explored; parameters that include erosion rate, incision magnitude, and topographic geometry. Synthetic canyon modeling has shown the nature and magnitude of each of these parameters on age distributions and can be used to optimize model parameters. In the second step, the erosion history is adjusted to minimize misfits between predicted and observed ages. Deceleration or acceleration of erosion rates are used to either increase or decrease predicted ages, respectively. Weighted chi^2 misfit is used to determine the degree of agreement of predicted with observed ages and models are iteratively modified to minimize the chi^2 misfit. Best fit erosion scenarios are finally compared with available

independent geological constraints to asses the viability of the best fit erosion model for each of the two end-member canyon cutting scenarios.

All modeled eastern Grand Canyon, erosion scenarios conform to the following boundary conditions that are independently constrained by geologic evidence, such as (1) the thickness of eroded section does not exceeding 4.5 km (Dumitru et al., 1994), (2) the presence or initiation of incision of the eastern Grand Canyon is required by 6 Ma, and (3) the final topographic expression for all erosion scenarios match the modern topography.

4.2.1 Early Canyon Results

Early Canyon landscape evolution scenarios are based on the early canyon end member erosion scenario (see fig 2a, section 2.2). These models require that the Kaibab transects samples cool in a setting that includes a paleotopographic canyon. Initial topographic expressions matched the modern topographic expression and assume steady-state topography during erosion throughout the model simulation. In this way, incision rates match erosion rates of the surrounding plateau.

The best fit erosion scenario produced a weighted chi² misfit of 0.79 (Fig. 11). This early canyon erosion scenario indicates that apparent erosion (and incision) rates overestimate true erosion rate by a factor of ~2x. The best fit true erosion rate is ~35 m/myr during the span of observed AHe ages (i.e. ~60-35 Ma). In addition, a post-35 Ma average erosion rate of ~35 m/myr is also needed to exhume the cooled samples to the modern surface. Incorporation of published apatite fission track data (Dumitru et al., 1994) requires increased erosion rates of ~100 m/myr prior to 60 Ma to produce predicted

apatite fission track ages that match the corrected fission track ages. Maximum allowed thickness of the eroded section suggests an onset of the erosion no earlier than ~84 Ma.

Modeling results for these non-smoothed topographic models also clearly show that small-scale topographic isotherm perturbation can be observed in predicted ages from ridges and drainages. For example, predicted ages from the South Kaibab traverse collected from along a ridge between two drainages, show a systematic deviation from linear age/elevation trends, giving older ages. In contrast, predicted ages from the North Kaibab transect collected along the Bright Angel drainage, show the opposite effect and deviate significantly from linearity, yielding younger ages. This systematic relationship is not apparent from the observed apatite (U-Th)/He data from neither transect in the eastern Grand Canyon.

4.2.2 Late Canyon Results

Late canyon erosion scenarios encompass all models where the Kaibab transect samples cool in a setting of low topographic relief, as defined by the late canyon end member erosion scenario (see figure 2b, section 2.2). After the closure of the samples, incision resulting in the eastern Grand Canyon is evoked. Because the youngest transect ages are latest Eocene, parameter exploration for the incision onset of the eastern Grand Canyon ranges from early Oligocene to Pliocene.

The late canyon best-fit erosion scenario produced a weighted chi² misfit of 0.24 and calls for middle-Cenozoic incision of the eastern Grand Canyon (see section 4.2.2.1). Synthetic Canyon modeling has shown that in scenarios of zero-relief, apparent erosion rates approximately equal true erosion (Fig. 12). The similar and linear distribution of

observed AHe ages from both transects is best modeled using an erosion rate of 75 m/myr from 55 Ma to 32 Ma, as directly constrained by the AHe data. Due to cooling in a low-relief setting predicted ages fall close to an average age/elevation trend, as predicted by synthetic canyon modeling. This pattern also closely matches the observed AHe data. Optimization of fit can be achieved by introducing a slightly lower erosion rate of 60 m/myr prior to 55 Ma, guided by the uppermost AHe data. This decreased erosion rate prior to 55 Ma also serves to produce predicted AFT ages without the further variation in erosion rates.

4.2.2.1 Evidence for an Oligocene Incision Event

Given the regional geothermal gradient (25°C/km), the depth below the modern canyon rim (1.6 km), and a mean annual surface temperature of 10±5°C, the lowermost transect samples would remain within the PRZ at temperatures of ~45-55°C in the absence of a canyon. Apatite grains that reside at this temperature still undergo enhanced He diffusion and would have not undergone complete age closure. The observed ages of ~35 Ma at the base of the transects then require the appearance of a canyon of roughly the same age in order to adequately cool samples and result in age closure. In Figure 12a, black circles representing modeled ages, show the effect of the continued diffusion for the lowermost samples in the absence of a canyon. Additionally, there appears to be no correlation between age and grain size for these lowermost samples (see appendix B). This indicates that the samples did not undergo extended periods of time in the PRZ, and therefore could not indicate earlier (~45-60 Ma) unroofing to the Kaibab limestone

surface followed by extended residence in the PRZ and eventual cooling through the PRZ due to a Pliocene or later incision event.

4.3 Discussion of Modeling Results

4.3.1 Early Canyon Discussion

The best fit early canyon erosion scenario dictates rapid erosion rates (100 m/my) in the late Mesozoic followed by relatively low erosion rates (35 m/my) throughout the vast majority of the Cenozoic. The accelerated erosion rates of the late Mesozoic are easily attributable to the broad upwarping of the plateau rim at the onset of the Laramide orogeny. The drop in erosion rate from 100 m/my to 35 m/my at roughly 60 Ma is necessary to explain both AHe and AFT data and is constrained to the 10 my time gap when the recording thermochronometer is changing from AFT the AHe. This scenario describes a Laramide unroofing schedule that is largely early-Laramide, with erosion rates dropping to background by the earliest Cenozoic. Although Cenozoic erosion rates are only directly constrained through the Eocene, an average post-Eocene erosion rate of 35 m/my is required to exhume samples to the surface by modern times. This rate is ~4x lower than the Pleistocene erosion rate of 144 m/my (Pederson et al., 2002a).

As synthetic canyon modeling has shown, a canyon on the scale of the modern Grand Canyon can result in observable changes in age distributions due to isotherm deflection. These effects of paleotopography can be seen in the calculated ages in figure 11a. The separation of ages from an average linear trend, as indicated by the arrows, is due to the differing transect geometries and the effects of the small scale topographic geometries that samples were collected on. This age separation lies just outside the error

of many of the samples and is not seen in the observed dataset. One might assume the presence of a more symmetric canyon at the time of sample cooling, to explain the lack of age separation between the observed dataset. However, this seems unlikely due to the observable age pattern that results from recent geometry changes (see section 3.2.2). In addition, the Bright Angel drainage is structurally controlled by the Laramide-aged Bright Angel Fault. It therefore stands to reason that such a topographic feature would be non-transient in nature.

4.3.2 Late Canyon Discussion

Late Canyon erosion scenarios assume sample cooling in a setting of low relief, followed by incision of the eastern Grand Canyon at some time after the closure of the lowermost samples (at 35 Ma). Best fit parameters dictate Oligocene incision of the Kaibab Uplift for reasons discussed in section 4.2.2.1. Removal of the Mesozoic overburden, as prescribed by the late canyon bet fit erosion scenario, also shows a strong unroofing event that is likely associated with Laramide orogeny. Moderate erosion rates of the latest Cenozoic (60 m/my) are slightly accelerated in the Eocene (~75 m/my), indicating continued unroofing in the late Laramide. Eocene formation of the Kaibab Uplift has been previously speculated (Young, 1979). Young (1979) describes Eocene-aged lacustrine deposits that rest on Kaibab limestone near Longs Point, in the western Grand Canyon, indicate early Cenozoic exposure of the modern Kaibab limestone erosion surface and compartmentalization east of the Kaibab Uplift. AFT data from the Grand Canyon also support an episode of exhumation in the Eocene attributed to formation of the Kaibab monocline (Naeser et al., 1989). Erosional style during cooling of the AHe

vertical transect samples, as defined by the erosional scenario, is low-relief. Synthetic canyon modeling has shown that samples cooled in such a setting exhibit highly linear age-invarient age/elevation relationships. For this reason, the highly linear nature of the observed AHe age/elevation trend is best modeled by cooling in a low-relief environment.

Due to the regional geothermal gradient (25°C/km) and typical average surface temperature (10°C), the depth associated with AHe age closure occurs at approximately the same stratigraphic depth of the lowermost transect samples. As a result, the AHe ages from the lowermost samples roughly represent a time of near exposure of the modern Kaibab Limestone erosion surface. For this reason, the large change in erosion rate (from 75 m/my to 0 m/my) occurs as the modern erosion surface is exposed and the lowermost samples are initially cooling. This event also temporally corresponds with the switch in erosional style from planation to localized incision soon after the exposure of the Kaibab Limestone surface. Partial deflection of the Colorado River around the Kaibab Uplift might indicate the planar interface between the newly exhumed Kaibab Uplift and the denuding Mesozoic strata at the time of incision.

4.3.3. Summary of Grand Canyon Modeling

Our modeling results show that both end-member erosional scenarios can be optimized to yield predicated ages within a reasonable fit of the observed thermochronometric data. However, the best-fit long-term landscape evolution model for the eastern Grand Canyon in terms of optimization of predicated and observed age patterns and in terms of agreement with independent geological constraints, the late

canyon model is preferred here. In this best-fit scenario, moderate erosion rates (~60 m/my) are accelerated to slightly higher rates (~75 m/my) during an Eocene erosion event most likely attributed to the late-Laramide formation of the Kaibab Uplift. Erosion during this was accomplished through low-relief planation. Subsequently, a change in late-Eocene to Oligocene erosion style results in localized incision and creation of a middle Cenozoic canyon spatially coincident with the eastern Grand Canyon soon after the exposure of the Kaibab Limestone. It should be noted that this incision is only constrained to the sample area atop the Kaibab Uplift and does not imply an incision history of the western Grand Canyon.

Despite the differences between the two best-fit erosion scenarios, the latest-Eocene ages for the lowest transect samples requires the presence of a paleocanyon in the area of the eastern Grand Canyon by the late Oligocene, regardless of the preferred best-fit erosion scenario. This conclusion is supported by both of the best fit end member erosion scenarios, and by consideration of the geothermal gradient and diffusion parameters and observed late-Eocene AHe ages (see section 4.2.2.1). Unfortunately, the size of this middle-Cenozoic canyon is difficult to asses due to the dependence on accurate description of the diffusion parameters. However preliminary results indicate a canyon of no less than 0.75km depth to adequately cool the lowermost AHe transect samples and produce the observed late Eocene ages. Ongoing work is incorporating the diffusion parameters described by Shuster and others (2006), to more accurately constrain the evolution of this middle Cenozoic canyon.

5. Conclusions

Several theoretical, modeling, and applied thermochronometric studies have demonstrated that closure isotherm perturbation due to topographic cooling and thus the spatial distribution of low-temperature thermochronometric data can be inverted to provide constraints on long-term landscape evolution and paleo-topography.(eg House et al., 1997; Armstrong et al., 2003; Braun, 2005; Shuster et al., 2005) This study has utilized this numerical approach to investigate the resolvability of different idealized canyon cutting scenarios (e.g., relative timing, magnitude, and geometry) and combined with more realistic scenarios and low-temperature thermochronometric data from the eastern Grand Canyon to elucidate the erosion and incision history. The results demonstrate that thermo-kinetic modeling of synthetic and real landscape evolution scenarios applicable to the Grand Canyon can quantify topographically-induced age patterns and distinguish between different erosion/incision models. The results, however, also show that a range of possible landscape evolution histories can provide similar age patterns that are not resolvable given the uncertainties of low-temperature thermochronometry, but that can possibly distinguished through the incorporation of independent geologic constraints.

Specific investigation of the Grand Canyon thermochronometric data in a quantitative fashion exemplifies the variability in possible erosion/landscape evolution scenarios. Substantial differences in prescribed histories for each of the end-member erosion scenarios outline the importance for considering the influence topography on isotherm perturbation and thermochronometric age distribution. Careful quantitative treatment and systematic sample collection allow identification of paleotopographic

signatures and quantification the paleo-relief and long-term landscape evolution from low-temperature thermochronometric data. In the eastern Grand Canyon, the lack of detectable isotherm deflection in the Kaibab vertical transects indicates cooling and erosional exhumation in a low-relief setting in post-Laramide times. However, latest Eocene to early Oligocene ages from the base of the Grand Canyon and systematic numerical modeling point to the cutting of a paleo-canyon soon after the exposure of the modern erosion surface defined by the Kaibab Limestone at 35-25 Ma. The existence of an ancestral eastern Grand Canyon in the Oligocene also provides a model for explaining the modern course of the Colorado River through the region.

However, more work is needed to more accurately and rigorously describe the Cenozoic landscape evolution of the eastern Grand Canyon, the Kaibab uplift, and surrounding area. Diffusion parameters incorporating alpha-radiation enhanced retentivity (Shuster et al., 2006) will be modeled to asses the effect of alpha-radiation damage on synthetic and real datasets. In addition, future sensitivity analysis of diffusion parameters and thermophysical parameters will provide rigorous limits for possible erosion scenario variability. Finally, near-horizontal transect samples collected from the Colorado River are currently being investigated to asses the lateral patterns of erosion along the course of the entire Grand Canyon. Spatial variation in cooling histories should help identify and constrain Laramide unroofing patterns and middle Cenozoic erosion processes and drainage evolution.

REFERENCES CITED

Armstrong, P.A., Ehlers, T.A., Chapman, D.S., Farley, K.A., and Kamp, P.J.J., 2003, Exhumation of the central Wasatch Mountains, Utah; 1, Patterns and timing of exhumation deduced from low-temperature thermochronology data: Journal of Geophysical Research, B, Solid Earth and Planets.

Beus, S.S., and Morales, M., 2003, Introducing the Grand Canyon.; 2.; Grand Canyon geology, p. 1-8.

Bilodeau, W.L., 1986, The Mesozoic Mogollon Highlands, Arizona; an Early Cretaceous rift shoulder: Journal of Geology, v. 94, p. 724-735.

Braun, J., 2002, Quantifying the effect of Recent relief changes on age-elevation relationships: Earth and Planetary Science Letters, v. 200, p. 331-343.

—, 2003, Pecube; a new finite-element code to solve the 3D heat transport equation including the effects of a time-varying, finite amplitude surface topography: Computers and Geosciences, v. 29, p. 787-794.

—, 2005, Quantitative constraints on the rate of landform evolution derived from low-temperature thermochronology.; Low-temperature thermochronology; techniques, interpretations, and applications: Reviews in Mineralogy and Geochemistry, v. 58, p. 351-374.

Brown, R.W., Cockburn, H.A.P., Kohn, B.P., Belton, D.X., Fink, D., Gleadow, A.J.W., and Summerfield, M.A., 2002, Combining low temperature apatite thermochronology and cosmogenic isotope analysis in quantitative landscape evolution studies.; Abstracts of the 12th annual V. M. Goldschmidt conference: Geochimica et Cosmochimica Acta, v. 66, p. 106.

Burchfiel, B.C., Cowan Darrel, S., and Davis Gregory, A., 1992, Tectonic overview of the Cordilleran Orogen in the Western United States.; The Cordilleran Orogen; conterminous U.S.; The geology of North America. 1992, p. 407-479.

Castor, S.B., and Faulds, J.E., 2000, Post-6 Ma limestone along the southeastern part of the Las Vegas Valley shear zone, southern Nevada.; Colorado River origin and evolution; proceedings of a symposium, p. 77-79.

Clark, M.K., House, M.A., Royden, L.H., Whipple, K.X., Burchfiel, B.C., Zhang, X., and Tang, W., 2005, Late Cenozoic uplift of southeastern Tibet: Geology (Boulder), v. 33, p. 525-528.

Condie, K.C., and Selverstone, J., 1999, The crust of the Colorado Plateau; new views of an old arc: Journal of Geology, v. 107, p. 387-397.

Dumitru, T.A., Duddy, I.R., and Green, P.F., 1994, Mesozoic-Cenozoic burial, uplift, and erosion history of the west-central Colorado Plateau; with Suppl. Data 9428: Geology (Boulder), v. 22, p. 499-502.

Ehlers, T.A., 2005, Crustal thermal processes and the interpretation of thermochronometer data.; Low-temperature thermochronology; techniques, interpretations, and applications: Reviews in Mineralogy and Geochemistry, v. 58, p. 315-350.

Ehlers, T.A., and Chapman, D.S., 1999, Normal fault thermal regimes; conductive and hydrothermal heat transfer surrounding the Wasatch Fault, Utah: Tectonophysics, v. 312, p. 217-234.

Ehlers, T.A., Chaudhri, T., Kumar, S., Fuller, C.W., Willett Sean, D., Ketcham Richard, A., Brandon Mark, T., Belton David, X., Kohn Barry, P., Gleadow Andrew, J.W., Dunai Tibor, J., and Fu Frank, Q., 2005, Computational tools for low-temperature thermochronometer interpretation.; Low-temperature thermochronology; techniques, interpretations, and applications: Reviews in Mineralogy and Geochemistry, v. 58, p. 589-622.

Ehlers, T.A., and Farley, K.A., 2003, Apatite (U-Th)/ He thermochronometry; methods and applications to problems in tectonic and surface processes: Earth and Planetary Science Letters, v. 206, p. 1-14.

Ehlers, T.A., Farley, K.A., Rusmore, M.E., and Woodsworth, G.J., 2006, Apatite (U-Th)/ He signal of large-magnitude accelerated glacial erosion, southwest British Columbia: Geology (Boulder), v. 34, p. 765-768.

Farley, K.A., 2000, Helium diffusion from apatite; general behavior as illustrated by Durango fluorapatite: Journal of Geophysical Research, B, Solid Earth and Planets, v. 105, p. 2903-2914.

Farley, K.A., Wolf, R.A., and Silver, L.T., 1996, The effects of long alpha-stopping distances on (U-Th)/He ages: Geochimica et Cosmochimica Acta, v. 60, p. 4223-4229.

Faulds, J.E., Price, L.M., and Wallace, M.A., 2000a, Pre-Colorado River paleogeography and extension along the Colorado Plateau-Basin and Range boundary, northwestern Arizona.; Colorado River origin and evolution; proceedings of a symposium, p. 93-99.

Faulds, J.E., Wallace, M.A., Gonzales, L.A., and Heizler, M.T., 2000b, Depositional environment and paleogeographic implications of the late Miocene Hualapai Limestone, northwestern Arizona and southern Nevada.; Colorado River origin and evolution; proceedings of a symposium, p. 81-87.

Flowers, R.M., Shuster, D.L., Wernicke, B.P., and Farley, K.A., 2007, Radiation damage control on apatite (U-Th)/ He dates from the Grand Canyon region, Colorado Plateau: Geology (Boulder), v. 35, p. 447-450.

Haeuselmann, P., Granger, D.E., Jeannin, P.Y., and Lauritzen, S.E., 2007, Abrupt glacial valley incision at 0.8 Ma dated from cave deposits in Switzerland: Geology (Boulder), v. 35, p. 143-146.

House, M.A., Wernicke, B.P., Farley, K.A., and Dumitru, T.A., 1997, Cenozoic thermal evolution of the central Sierra Nevada, California, from (U-Th)/ He thermochronometry: Earth and Planetary Science Letters, v. 151, p. 167-179.

Karlstrom, K.E., Ilg, B.R., Williams, M.L., Hawkins, D.P., Bowring, S.A., and Seaman, S.J., 2003, Paleoproterozoic rocks of the Granite Gorges.; 2.; Grand Canyon geology, p. 9-38.

Kelley, S.A., Chapin, C.E., and Karlstrom, K.E., 2000, Laramide cooling histories of Grand Canyon, Arizona, and the Front Range, Colorado, determined from apatite fission-track thermochronology.; Colorado River origin and evolution; proceedings of a symposium, p. 37-41.

Mancktelow, N.S., and Grasemann, B., 1997, Time-dependent effects of heat advection and topography on cooling histories during erosion: Tectonophysics, v. 270, p. 167-195.

Naeser, C.W., Duddy, I.R., Elston, D.P., Dumitru, T.A., and Green, P.F., 1989, Fission-track dating; ages for Cambrian strata; and Laramide and post-middle Eocene cooling events from the Grand Canyon, Arizona.; Geology of Grand Canyon, northern Arizona (with Colorado River guides); Lees Ferry to Pierce Ferry, Arizona.; Field trips for the 28th international geological congress. 1989, p. 139-144.

Pederson, J., Karlstrom, K., Sharp, W., and McIntosh, W., 2002a, Differential incision of the Grand Canyon related to Quaternary faulting--Constraints from U-series and Ar/Ar dating: Geology, v. 30, p. 739-742.

Pederson, J.L., 2000, Searching for the pre-Grand Canyon Colorado River; the Muddy Creek Formation north of Lake Mead.; Colorado River origin and evolution; proceedings of a symposium, p. 71-75.

Pederson, J.L., Mackley, R.D., and Eddleman, J.L., 2002b, Colorado Plateau uplift and erosion evaluated using GIS: GSA Today, v. 12, p. 4-10.

Reiners, O.W., Ehlers, T.A., Mitchell, S.G., and Montgomery, D.R., 2003, Coupled spatial variations in precipitation and long-term erosion rates across the Washington Cascades: Nature (London), v. 426, p. 645-647.

Reiners, P.W., and Farley, K.A., 2001, Influence of crystal size on apatite (U-Th)/ He thermochronology; an example from the Bighorn Mountains, Wyoming: Earth and Planetary Science Letters, v. 188, p. 413-420.

Roy, M., Kelley, S., Pazzaglia, F.J., Cather, S., and House, M.A., 2004, Middle Tertiary buoyancy modification and its relationship to rock exhumation, cooling, and subsequent extension at the eastern margin of the Colorado Plateau: Geology (Boulder), v. 32, p. 925-928.

Schlunegger, F., and Willett, S.D., 1999, Spatial and temporal variations in exhumation of the central Swiss Alps and implications for exhumation mechanisms.; Exhumation processes; normal faulting, ductile flow and erosion: Geological Society Special Publications, v. 154, p. 157-179.

Shuster, D.L., Ehlers, T.A., Rusmore, M.E., and Farley, K.A., 2005, Rapid glacial erosion at 1.8 Ma revealed by (super 4) He/ (super 3) He thermochronometry: Science, v. 310, p. 1668-1670.

Shuster, D.L., Flowers, R.M., and Farley, K.A., 2006, The influence of natural radiation damage on helium diffusion kinetics in apatite: Earth and Planetary Science Letters, v. 249, p. 148-161.

Stock, G.M., Anderson, R.S., and Finkel, R.C., 2004, Pace of landscape evolution in the Sierra Nevada, California, revealed by cosmogenic dating of cave sediments: Geology (Boulder), v. 32, p. 193-196.

Stockli, D.F., 2005, Application of low-temperature thermochronometry to extensional tectonic settings.; Low-temperature thermochronology; techniques, interpretations, and applications: Reviews in Mineralogy and Geochemistry, v. 58, p. 411-448.

Stockli, D.F., Farley, K.A., Dumitru, T.A., and Anonymous, 2000, Intercalibration and integration of apatite (U-Th)/ He and fission track thermochronometers on an exhumed extensional fault block, White Mountains, eastern California, U.S.A.; Fission track 2000; 9th international conference on fission track dating and thermochronology: Abstracts Geological Society of Australia, v. 58, p. 305-307.

Stuewe, K., White, L., and Brown, R., 1994, The influence of eroding topography on steady-state isotherms; application to fission track analysis: Earth and Planetary Science Letters, v. 124, p. 63-74.

Whipp, D.M., Jr., and Ehlers, T.A., 2007, Influence of groundwater flow on thermochronometer-derived exhumation rates in the central Nepalese Himalaya: Geology, v. 35, p. 851-854.

Whipple, K.X., Kirby, E., and Brocklehurst, S.H., 1999, Geomorphic limits to climate-induced increases in topographic relief: Nature (London), v. 401, p. 39-43.

Whipple, K.X., and Meade, B.J., 2004, Controls on the strength of coupling among climate, erosion, and deformation in two-sided, frictional orogenic wedges at steady state: Journal of Geophysical Research, F.

Young, R.A., 1979, Laramide deformation, erosion and plutonism along the southwestern margin of the Colorado Plateau.; Plateau uplift; mode and mechanism: Tectonophysics, v. 61, p. 25-47.

—, 2000, The Laramide-Paleogene history of the western Grand Canyon region; setting the stage.; Colorado River origin and evolution; proceedings of a symposium, p. 7-15.

LIST OF FIGURES AND TABLES

Table 1. Summary of Thermophysical and Spatial Model Parameters

Parameter	Value	Units
Thermophysical Parameters		
Thermal diffusivity	34.1*	(km²/Myr)
Base Temperature	686*	(ºC)
Surface temperature	10	(ºC)
Lapse rate	none	(C/km)
Heat production	0.97*	(C/My)
Spatial Parameters		
Surface Node Spacing	261	(m)
Isostatic compensation	no	-
Model thickness	40	(km)
Number of z-node planes	41	-

*see appendix A for justification

Table 2. Apatite (U-Th)/He Data Summary

Sample	mean age (My)	error (My)*	# of analyses	mean [eU] (ppm)	mean FT	elevation (m)	rock unit
South Kaibab Transect							
GCSK 1	51.8	9.0	5	47	0.61	2164	Kaibab Fm
GCSK 2	50.2	5.3	4	43	0.61	2073	Toroweap Fm
GCSK 3	48.4	4.8	4	23	0.61	1951	Coconino ss
GCSK 4	48.5	2.5	7	44	0.63	1920	Coconino ss
GCSK 5	60.9	7.5	3	38	0.55	1902	Coconino ss
GCSK 6	49.4	3.7	5	66	0.61	1829	Esplanade ss
GCSK 7	40.5	10.7	4	54	0.68	1756	Supai Grp
GCSK 8	66.1	5.2	3	31	0.56	1682	Supai Grp
GCSK 9	45.3	6.3	5	43	0.48	1646	Supai Grp
GCSK 10	41.2	4.4	4	39	0.60	1207	Tapeats ss
GCSK 12	39.4	9.6	4	38	0.68	1033	Bass Fm
GCSK 13	37.3	15.1	2	14	0.60	944	Vishnu Schist
GCSK 15	60.6	3.8	9	25	0.72	818	Brahma Schist
GCSK 16	36.8	5.3	2	7	0.74	758	Vishnu Schist
North Kaibab Transect							
GCNK 1	59.8	7.8	4	25	0.65	2391	Toroweap Lm
GCNK 2	57.9	4.8	5	47	0.66	2309	Coconino ss
GCNK 4	53.0	7.4	5	71	0.63	1999	Supai ss
GCNK 9	41.3	12.1	3	19	0.63	993	Vishnu Schist
GCNK 10	45.7	5.2	6	4	0.76	944	Rama Schist
GCNK 11	40.3	6.3	1	9	0.75	896	Vishnu Schist
GCNK 12	39.7	2.6	4	3	0.78	843	Vishnu Schist

* Errors with fewer than four analyses are standard deviation. Errors with 4 or more analyses are standard errors ($\sigma/\sqrt{n}$)

Table 3. Complete Kiabab Transect (U-Th)/He Data

	Aliquot Measurements								Sample Averages		
Sample	Age [Ma]	± [Ma]	U [ppm]	Th [ppm]	Sm [ppm]	eU	He [ncc/mg]	Ft	Age (Ma)	±** (Ma)	#
GCSK1	27.3	1.4	21.2	36.8	-	30	56.8	0.57	**51.8**	**9.0**	**5**
GCSK1	47.9	2.4	25.6	63.4	-	41	129.8	0.55			
GCSK1*	21.1	1.1	10.5	14.8	-	14	21.9	0.61			
GCSK1	57.3	2.9	32.4	30.1	-	39	200.6	0.73			
GCSK1	66.7	4.0	66.6	1.3	24.2	67	15.72	0.65			
GCSK1	59.7	3.6	57.1	14.8	77.9	61	11.08	0.56			
GCSK2	61.8	3.1	24.5	155.2	-	61	259.3	0.56	**50.2**	**5.3**	**4**
GCSK2	43.3	2.2	24.3	24.0	-	30	100.7	0.64			
GCSK2	39.4	2.0	20.5	70.8	-	37	108.9	0.61			
GCSK2	56.2	2.8	34.7	43.9	-	45	191.0	0.62			
GCSK3	40.4	2.0	20.9	108.5	-	46	121.6	0.53	**48.4**	**4.8**	**4**
GCSK3	50.5	2.5	13.9	85.0	-	34	135.2	0.65			
GCSK3	61.0	3.0	2.8	19.8	-	7	32.9	0.60			
GCSK3	41.6	2.1	1.2	12.0	-	4	13.7	0.67			
GCSK4	49.6	2.5	14.4	38.6	-	24	90.1	0.63	**48.5**	**2.5**	**7**
GCSK4	52.7	2.6	115.1	156.3	-	152	621.7	0.64			
GCSK4	46.8	2.3	26.7	66.1	-	42	155.6	0.65			
GCSK4	39.2	2.35	4.4	18.9	340.2	9	37.6	0.68			
GCSK4	52.6	3.15	11.0	44.4	104.7	21	89.1	0.62			
GCSK4	40.6	2.43	14.7	30.6	515.1	22	75.9	0.59			
GCSK4	57.7	3.46	33.0	18.0	210.9	37	173.4	0.63			
CGSK5	55.7	2.8	39.7	40.2	-	49	184.2	0.55	**60.9**	**7.5**	**3**
CGSK5	69.5	3.5	40.1	16.9	-	44	212.0	0.57			
GCSK5*	71.4	1.6	51.9	136.0	224.5	84	19.80	0.60			
GCSK5*	79.5	1.6	75.9	287.3	333.4	143	37.00	0.59			
GCSK5	57.6	2.4	16.8	17.3	95.0	21	3.67	0.54			
GCSK6	53.6	2.7	39.8	86.3	-	60	243.3	0.62	**49.4**	**3.7**	**5**
GCSK6	41.2	2.1	7.5	71.1	-	24	73.9	0.61			
GCSK6	56.2	3.37	9.7	38.0	159.6	19	96.4	0.70			
GCSK6	56.2	3.37	75.2	387.0	797.8	166	685.1	0.58			
GCSK6	39.6	2.37	33.7	111.1	104.4	60	161.1	0.55			
GCSK7	27.9	1.4	12.8	171.0	-	53	119.4	0.66	**40.5**	**10.7**	**4**
GCSK7	40.4	2.0	43.8	203.9	-	92	276.1	0.61			
GCSK7	23.1	1.2	13.2	167.3	-	53	102.8	0.70			
GCSK7	70.6	4.23	16.5	11.3	160.1	19	129.9	0.74			
GCSK8	72.1	4.3	20.1	25.1	41.3	26	6.33	0.61	**66.1**	**5.2**	**3**
GCSK8*	116.9	7.0	17.9	11.1	161.4	20	7.57	0.55			
GCSK8	62.5	3.8	29.4	58.4	187.1	43	8.70	0.57			
GCSK8*	92.7	5.6	4.4	13.2	61.0	8	2.07	0.51			
GCSK8	63.8	3.8	15.4	35.0	229.1	24	4.40	0.50			
GCSK9	44.5	2.7	14.5	78.9	53.9	33	90.5	0.50	**45.3**	**6.3**	**5**
GCSK9	69.9	4.2	20.5	66.6	306.9	36	167.3	0.51			
GCSK9	37.4	2.2	31.2	125.4	90.9	61	127.6	0.46			
GCSK9*	27.1	1.6	15.8	73.8	27.9	33	46.5	0.42			
GCSK9	37.2	2.2	16.3	62.1	181.0	31	65.2	0.44			
GCSK9	37.3	2.2	34.2	92.1	61.9	56	121.0	0.47			
GCSK10	35.4	1.8	37.3	139.4	-	70	180.9	0.60	**41.2**	**4.4**	**4**
GCSK10	51.9	2.6	18.9	17.5	-	23	87.0	0.60			
GCSK10	44.6	2.2	23.8	87.4	-	44	134.2	0.56			
GCSK10	32.8	1.6	13.3	27.7	-	20	52.8	0.67			
GCSK12	60.3	3.0	42.5	68.6	-	59	259.2	0.60	**39.4**	**9.6**	**4**
GCSK12	22.2	1.1	8.3	57.8	-	22	38.5	0.65			
GCSK12*	12.0	0.6	1.7	20.7	-	6.5	6.5	0.68			
GCSK12	50.9	2.5	39.8	36.7	-	48	210.5	0.70			
GCSK12	24.1	1.2	19.7	18.7	-	24	53.4	0.76			
GCSK12*	31.6	1.6	2.2	15.0	-	5.7	16.4	0.75			

Table 3 continued...

	Aliquot Measurements								Sample Averages		
Sample	Age [Ma]	± [Ma]	U [ppm]	Th [ppm]	Sm [ppm]	eU	He [ncc/mg]	Ft	Age (Ma)	±** (Ma)	#
GCSK13*	25.6	1.5	3.2	16.5	41.7	7.1	13.7	0.59	**37.3**	**15.1**	**2**
GCSK13	48.0	2.9	17.4	7.1	219.7	19	80.1	0.66			
GCSK13	26.6	1.6	5.3	12.4	45.1	8	15.0	0.54			
GCSK15	43.0	2.1	34.1	21.5	-	39	136.1	0.66	**60.6**	**3.8**	**9**
GCSK15	51.8	2.6	44.2	27.1	-	51	221.7	0.69			
GCSK15	55.4	2.8	18.3	10.7	-	21	104.8	0.74			
GCSK15	77.1	3.9	16.9	9.6	-	19	147.0	0.81			
GCSK15	60.7	3.64	25.7	13.6	568.5	29	179.7	0.72			
GCSK15	61.9	3.72	23.1	13.2	454.5	26	168.9	0.75			
GCSK15	75.5	4.53	9.2	4.2	292.4	10	87.5	0.76			
GCSK15	52.4	3.14	13.1	6.1	383.0	15	82.4	0.73			
GCSK15	67.7	4.06	9.8	6.7	262.0	11	69.9	0.62			
GCSK16*	17.8	0.9	3.6	15.0	-	7.1	9.9	0.64	**36.8**	**5.3**	**2**
GCSK16	33.0	1.7	5.3	6.5	-	7	20.6	0.75			
GCSK16	40.5	2.0	6.4	5.2	-	8	27.5	0.73			
GCNK1	40.6	2.44	7.2	17.3	216.5	11	44.8	0.69	**59.8**	**7.8**	**4**
GCNK1	77.8	4.67	30.6	68.4	161.0	47	288.7	0.63			
GCNK1	64.8	3.89	6.9	55.9	79.3	20	101.8	0.62			
GCNK1	56.0	3.36	15.1	35.4	156.0	23	107.5	0.64			
GCNK2	71.1	4.26	19.5	38.8	111.0	29	185.4	0.72	**57.9**	**4.8**	**5**
GCNK2	44.2	2.65	6.9	20.8	112.0	12	40.4	0.59			
GCNK2	64.0	3.84	144.7	107.1	320.4	170	874.8	0.65			
GCNK2	60.2	3.61	13.4	3.7	159.2	14	78.5	0.69			
GCNK2	50.2	3.01	5.0	27.9	107.8	12	50.2	0.66			
GCNK4	60.9	3.65	13.2	98.1	101.7	36	173.4	0.63	**53.0**	**7.4**	**5**
GCNK4	69.9	4.19	168.0	129.9	358.8	198	1071.6	0.62			
GCNK4	63.4	3.80	17.9	131.3	444.4	49	252.4	0.62			
GCNK4	36.9	2.21	10.9	143.9	247.3	45	132.6	0.63			
GCNK4	33.7	2.02	2.4	97.5	48.7	25	67.4	0.64			
GCNK9	48.3	2.90	23.1	2.4	66.4	24	94.2	0.66	**41.3**	**12.1**	**3**
GCNK9	27.3	1.64	19.0	4.5	118.6	20	47.0	0.67			
GCNK9	48.3	2.90	7.4	20.4	59.8	12	42.7	0.57			
GCNK10	32.8	1.97	3.2	0.8	131.8	3	13.4	0.76	**45.7**	**5.2**	**6**
GCNK10	66.1	3.97	4.9	1.2	176.8	5	40.7	0.77			
GCNK10	41.1	2.47	2.3	0.5	111.4	2	12.7	0.77			
GCNK10	42.2	2.53	3.8	0.9	149.0	4	20.1	0.75			
GCNK10	55.6	3.33	2.8	0.7	108.3	3	19.6	0.76			
GCNK10	36.3	2.18	3.4	1.0	163.4	4	16.1	0.73			
GCNK11	40.3	2.42	8.2	3.4	49.3	9	34.6	0.75	**40.3**	**6.3**	**1**
GCNK12	40.7	2.44	2.8	1.0	128.8	3	16.6	0.81	**39.7**	**2.6**	**4**
GCNK12	46.7	2.80	2.8	0.5	114.1	3	17.9	0.81			
GCNK12	35.7	2.14	2.8	0.8	134.7	3	12.9	0.73			
GCNK12	35.7	2.14	3.9	0.8	177.3	4	18.8	0.77			

* not included in sample averages

**errors with fewer than four analyses are standard deviation. Errors with 4 or more analyses are standard errors ($\sigma/\sqrt{n}$)

Figure 1.1. A colored-relief map from SRTM 90m DEM of the Eastern Grand Canyon showing transect sample location and the Kaibab Uplift. The inset shows regional location of the study.

Eastern Grand Canyon, Arizona

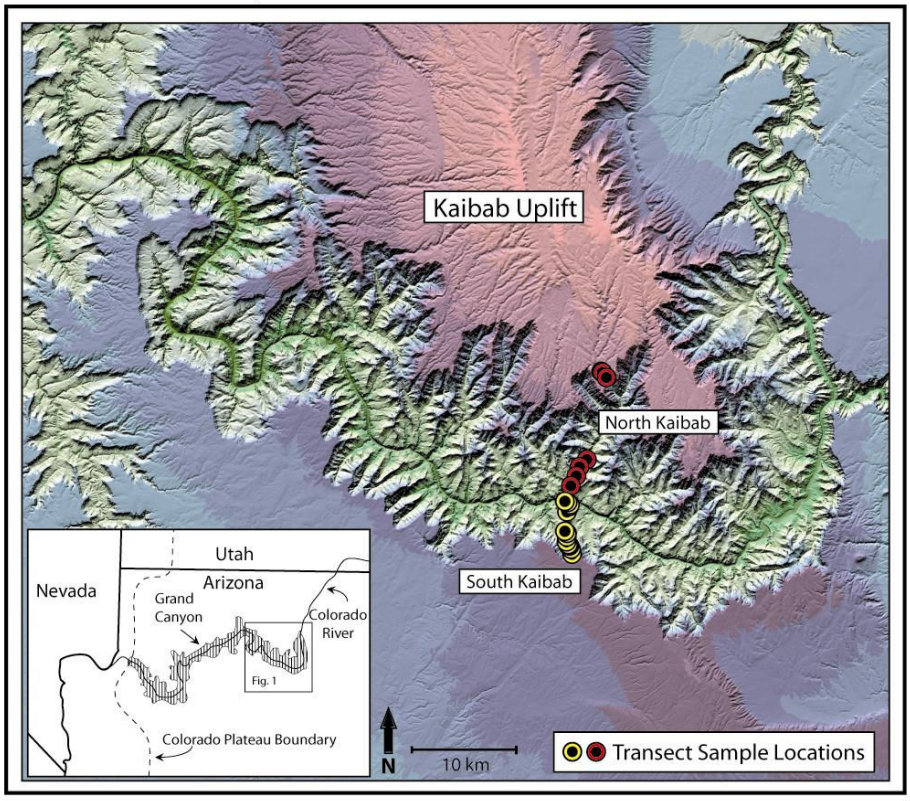

Figure 1.2. Generalized end-member erosion scenarios used in the study. A) Recent Canyon erosion scenarios assume low-relief topography through the erosion history followed by recent canyon formation (<30mya). B) Early Canyon erosion scenarios assume the formation of significant paleotopography in the Laramide. Parameters exploration for both end-member erosion scenarios includes: erosion rate(s), timing of incision, and paleo-canyon size and geometry, including recent geometry changes

.

Generalized Erosion Scenarios

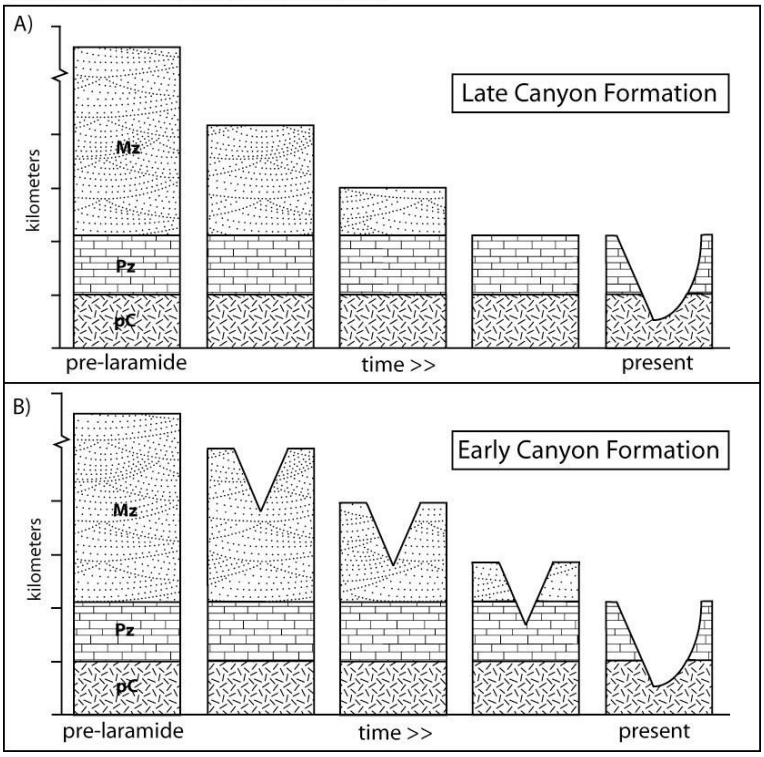

Figure 1.3. A) A schematic depiction of how negative, large-wavelength, topographic features can alter the age/elevation relationship due to deflection of isotherms. Age skewing is a function of the degree of isothermal deflection, geothermal gradient and surface temperature. B) Increasing age skewing towards the bottom of the transect leads to increased apparent erosion rates (Ea). Note that samples lying outside the region of isotherm deflection have unaltered ages. Therefore, the paleotopographic signature can be observed in samples collected outside the canyon itself.

Large Wavelength Topographic Effects

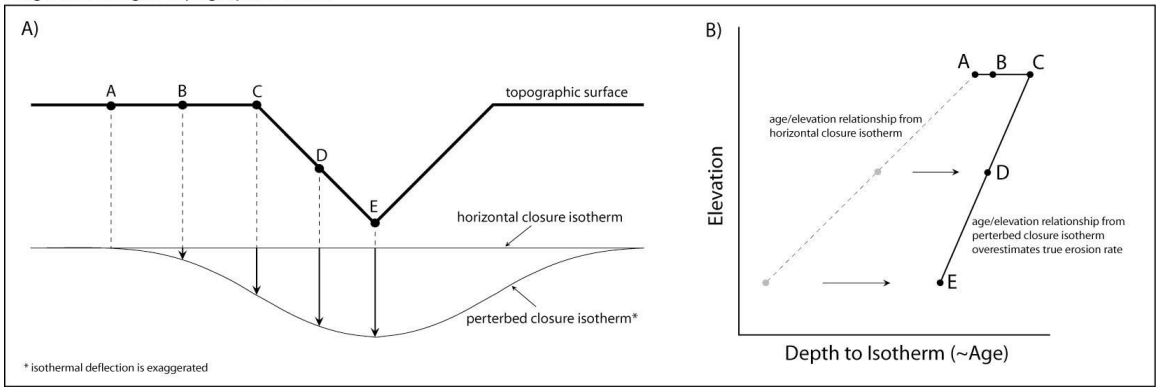

Figure 1.4. A) A profile view of a hypothetical canyon showing topography, perturbed isotherms, and sample locations. Isothermal perturbation is due to the large-wavelength topographic signature of the overall canyon. Small-wavelength topographic features, such as those at samples B and D, are not of enough size to significantly perturb the closure isotherm. Because isotherms are deflected, age/elevation data points also rely on lateral location with respect to the isotherms. B) Samples that lie near the average surface trend also lie near the average age/elevation trend. However, samples that lie off that average surface on topographic features that do not deflect the closure isotherm, age/elevation data points also deviate from the average age/elevation trend. Samples collected on short-wavelength topographic highs are skewed to older ages while samples collected on short-wavelength topographic lows are skewed to younger ages.

Short Wavelength Topographic Effects

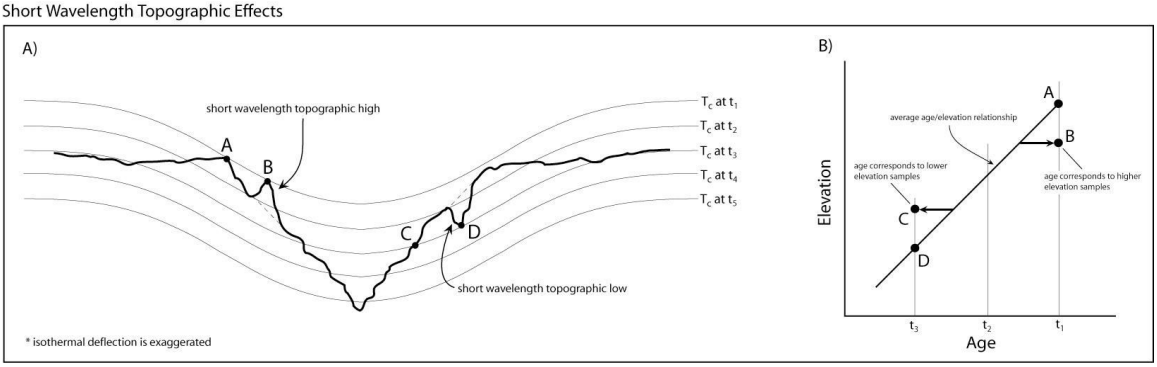

Figure 1.5. Crustal block inputs for synthetic and real canyon modeling. The thermophysical parameters for all of the models are listed in Table 1. A) 3-D perspectives of the model inputs shows the dimensions for each block. Because heat flow through block sides is zero (horizontal isotherms) model blocks must incorporate areas larger than the sample area to eliminate this edge effect. B) Canyon profiles for each of the model blocks.

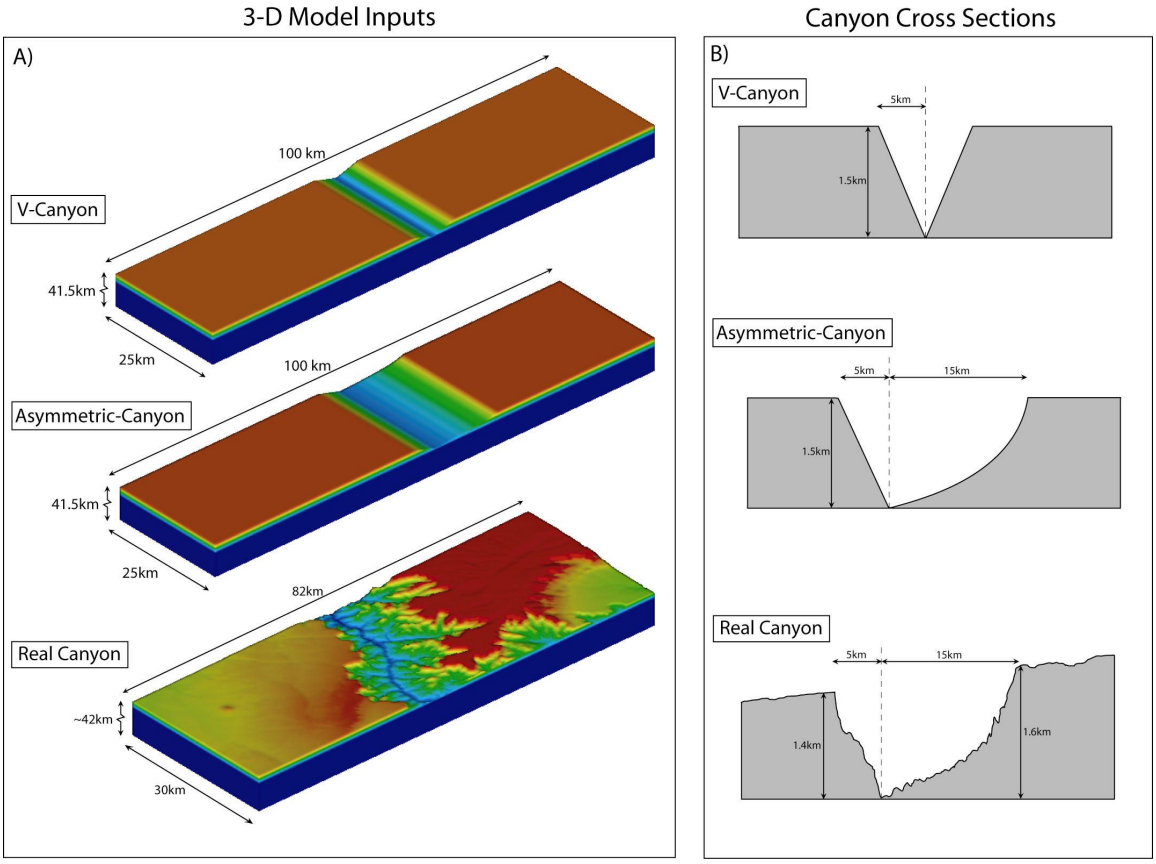
3-D Model Inputs
Canyon Cross Sections
A)
B)
V-Canyon
100 km
41.5km
25km
Asymmetric-Canyon
100 km
41.5km
25km
Real Canyon
82km
~42km
30km
V-Canyon
5km
1.5km
Asymmetric-Canyon
5km
15km
1.5km
Real Canyon
5km
15km
1.4km
1.6km

Figure 1.6. Comparative results from four erosion scenarios of the same erosion rate (Et=50m/my). A) and B) show results for *late* canyon erosion scenarios that end in v-canyon and symmetric-canyon geometries respectively. Age/elevation trends exhibit apparent erosion rates that closely match true erosion rates. Age profiles also show that samples cooled in zones of horizontal isotherms have age/invariant relationships; that is, ages do not depend on lateral position. C) and D) show results for *early* canyon erosions scenarios that also end in v-canyon and symmetric-canyon geometries respectively. However, age/elevation trends exhibit apparent erosion rates that are greater than true erosion rates. A loss of age/elevation invariance can be observed in both age/elevation plots and age profile plots. Note the diagnostic 'upwarping' of ages that occurs near the canyon edge.

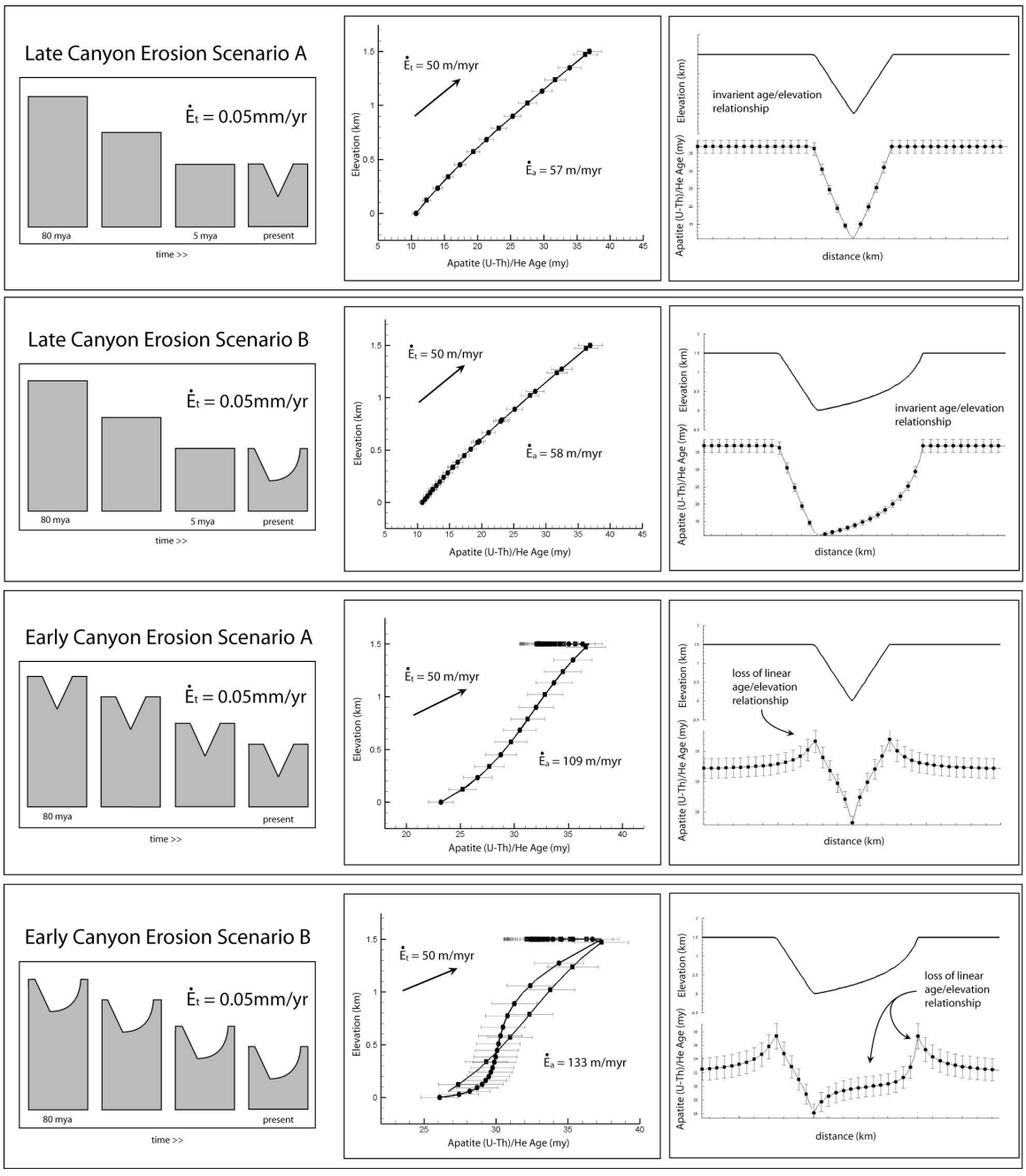
Late Canyon Erosion Scenario A
Ėt = 0.05mm/yr
80 mya
5 mya
present
time >>
Ėt = 50 m/myr
Ėa = 57 m/myr
Elevation (km)
Apatite (U-Th)/He Age (my)
invarient age/elevation relationship
Apatite (U-Th)/He Age (my)
distance (km)
Late Canyon Erosion Scenario B
Ėt = 0.05mm/yr
80 mya
5 mya
present
time >>
Ėt = 50 m/myr
Ėa = 58 m/myr
Elevation (km)
Apatite (U-Th)/He Age (my)
invarient age/elevation relationship
Apatite (U-Th)/He Age (my)
distance (km)
Early Canyon Erosion Scenario A
Ėt = 0.05mm/yr
80 mya
present
time >>
Ėt = 50 m/myr
Ėa = 109 m/myr
Elevation (km)
Apatite (U-Th)/He Age (my)
loss of linear age/elevation relationship
Apatite (U-Th)/He Age (my)
distance (km)
Early Canyon Erosion Scenario B
Ėt = 0.05mm/yr
80 mya
present
time >>
Ėt = 50 m/myr
Ėa = 133 m/myr
Elevation (km)
Apatite (U-Th)/He Age (my)
loss of linear age/elevation relationship
Apatite (U-Th)/He Age (my)
distance (km)

Figure 1.7. A contour plot illustrating the magnitude of difference between true erosion rate (Et) and apparent erosion rate (Ea) calculated using a symmetrical, v-shaped canyon of 10km width. The overestimation factor is calculated using the following equation: Fo = Ea/Et, where Fo is the overestimation factor. Ea and Et are the apparent and true erosion rates, respectively.

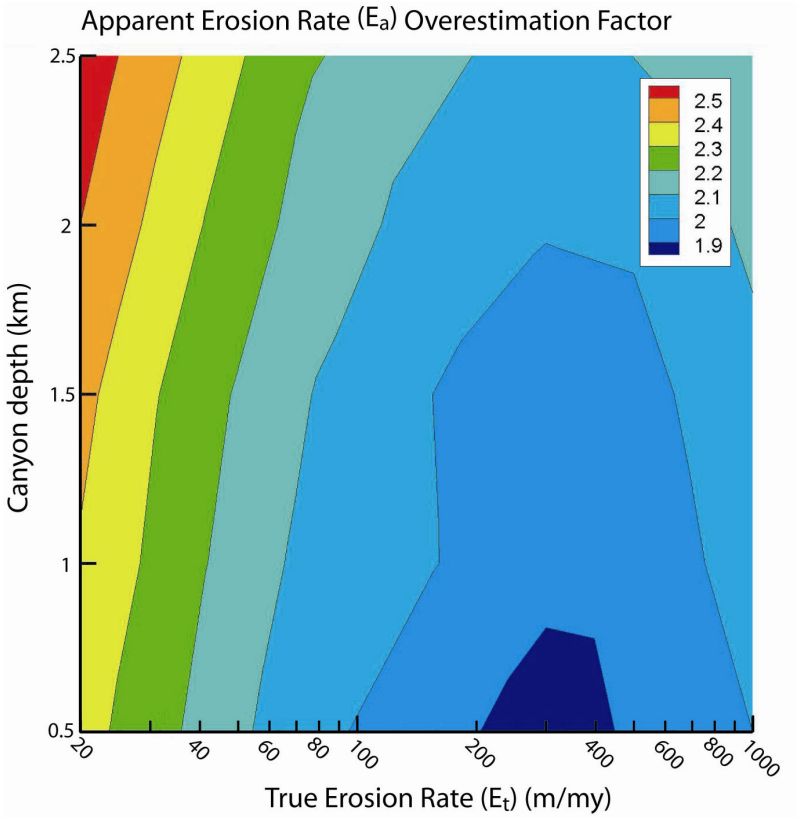
Apparent Erosion Rate (E_a) Overestimation Factor
Canyon depth (km)
2.5
2
1.5
1
0.5
2.5
2.4
2.3
2.2
2.1
2
1.9
20
40
60
80
100
200
400
600
800
1000
True Erosion Rate (E_t) (m/my)

Figure 1.8. The effects of recent geometry change on age data. A) The Age/Elevation plot for an erosion scenario prescribed by B). Note the large skewing of ages produced when younger samples are exhumed to the surface during relief change. C) An age profile showing the offset in ages relative to the canyon topography.

Effect of Recent Canyon Geometry Change

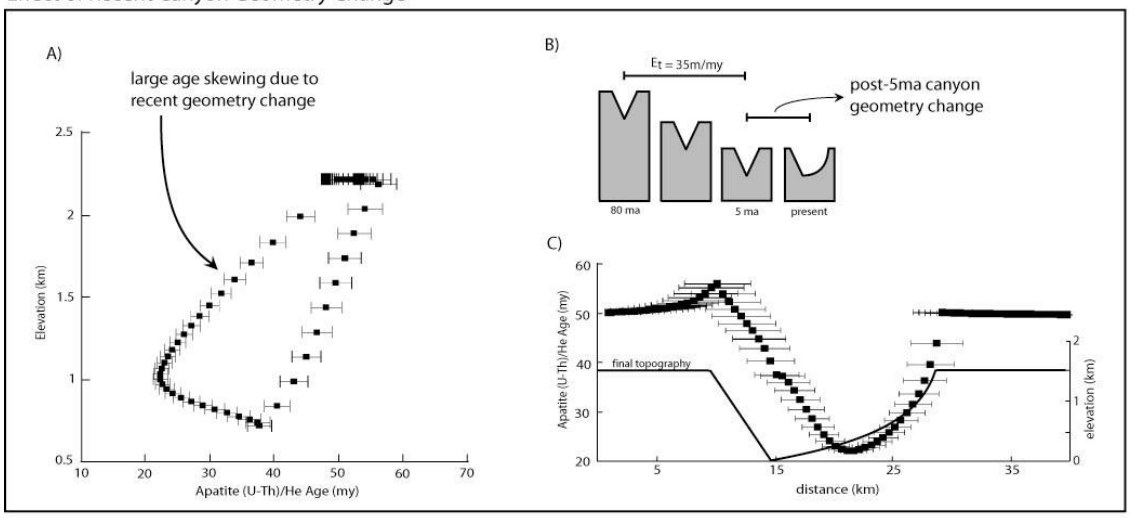

Figure 1.9. 3-D colored relief perspectives of each of the two transect locations, constructed from SRTM 90m data. A) The North Kaibab transect was collected along the axis of the Bright Angel drainage. The samples cover a lateral distance of 15km and a vertical difference of 1.6km B) The South Kaibab transect was collected along a drainage divide and spans a 5km lateral distance and 1.4km elevation differences.

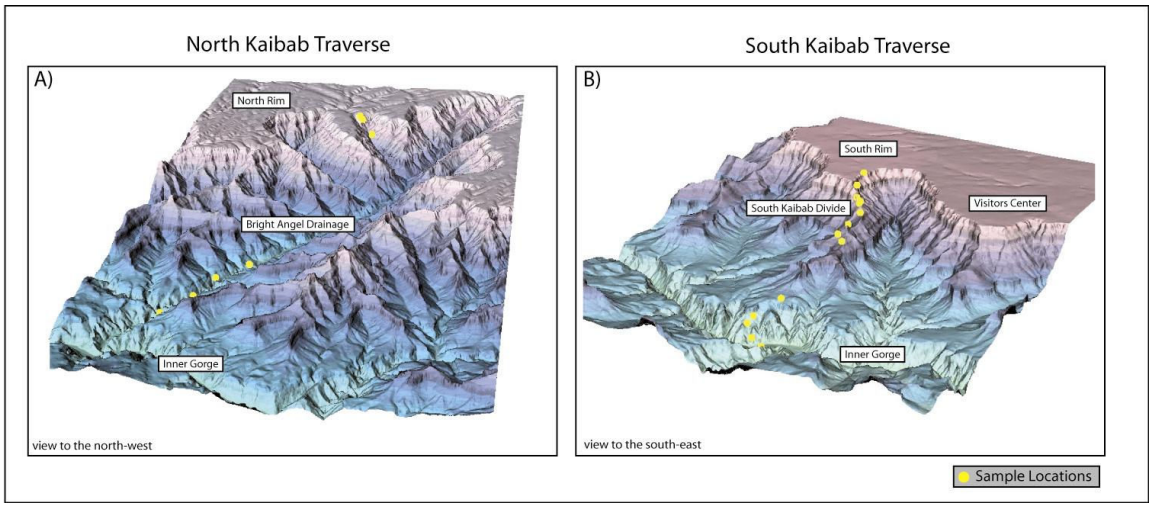
North Kaibab Traverse
A)
North Rim
Bright Angel Drainage
Inner Gorge
view to the north-west
South Kaibab Traverse
B)
South Rim
South Kaibab Divide
Visitors Center
Inner Gorge
view to the south-east
Sample Locations

Figure 1.10. Age/Elevation plots for the North (A) and South (B) Kaibab transects. Errors expressed are sigma (σ) for samples yielding <4 analysis and standard errors ($\sigma\sqrt{n}$) for samples yielding ≥4 analysis. Three outliers, most likely due to U/Th rich inclusions, are disregarded when calculating model misfit. Data exhibits a highly linear trend and the two transect trends overlap in error.

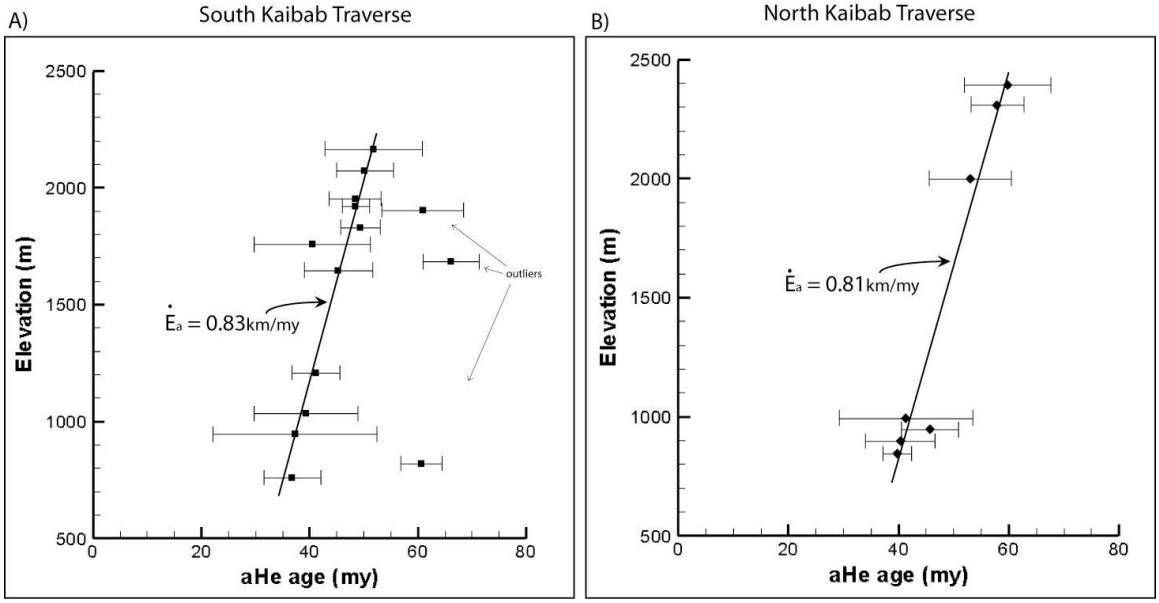
A)
South Kaibab Traverse
Elevation (m)
aHe age (my)
$\dot{E}_a$ = 0.83km/my
outliers
B)
North Kaibab Traverse
Elevation (m)
aHe age (my)
$\dot{E}_a$ = 0.81km/my

Figure 1.11. A) An age/elevation plot with observed and modeled data points for the best fit, early canyon, thermal history. The effect of short-wavelength topography on deflected isotherm isotherm scenarios can be seen by the separation of ages for the modeled North and South Kaibab transects. B) The prescribed thermal history for best fit parameters, and the resulting history of Mesozoic unroofing. A high rate of erosion in the early Laramide is followed by a relatively low erosion rate of 35m/my throughout the middle and late Cenozoic. Exposure of the modern Kaibab Limestone erosion surface occurs recently.

Early Canyon Model Results

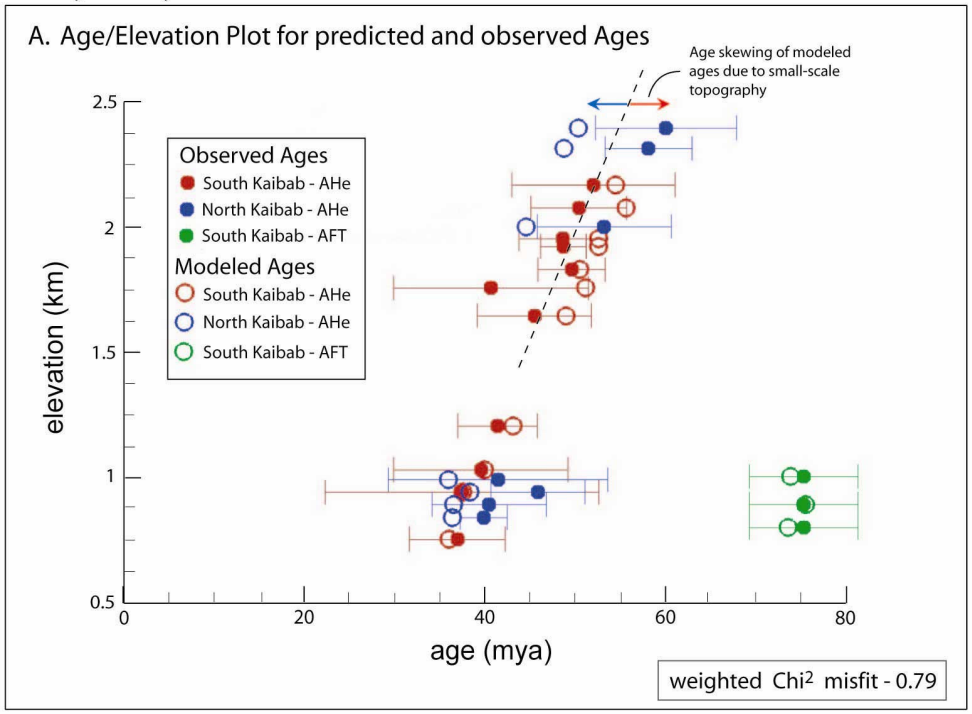

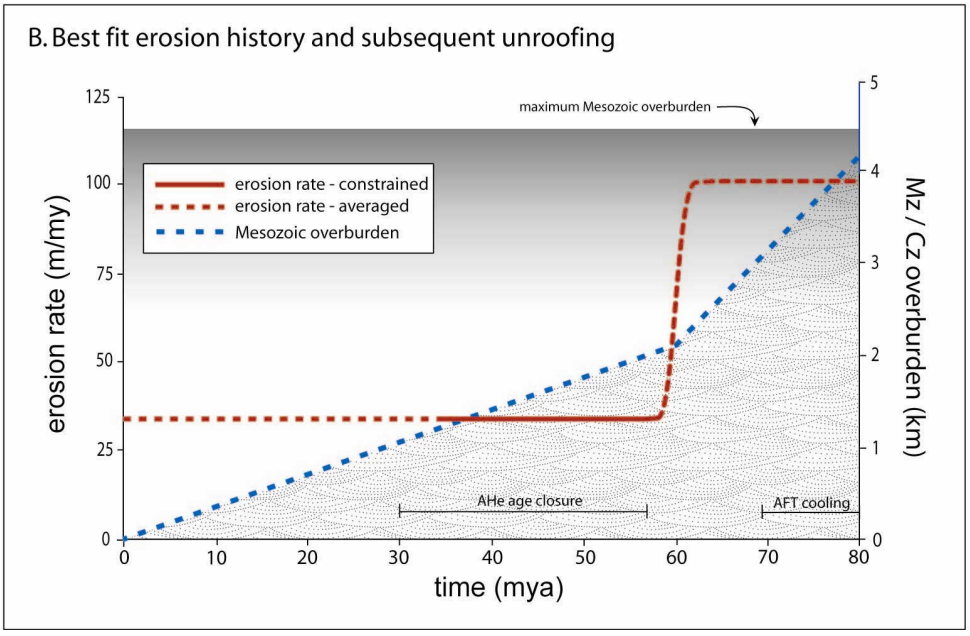

Figure 1.12. A) An age/elevation plot with observed and modeled data points for the best fit, recent canyon, thermal history. Cooling of samples under a low-relief surface results in a highly linear age/elevation trend of modeled data that closely matches observed data. B) The best-fit erosion history and resulting history of Mesozoic unroofing. Only a slight increase in the erosion rate in the early Laramide is needed to produce matched AFT ages. An erosion rate of 75m/my during the Paleocene results in the early (~30ma) exposure of the modern Kaibab Limestone erosion surface. Incision of a Miocene paleocanyon is required to preserve late Eocene AHe ages.

Late Canyon Model Results

A. Age/Elevation Plot for predicted and observed Ages

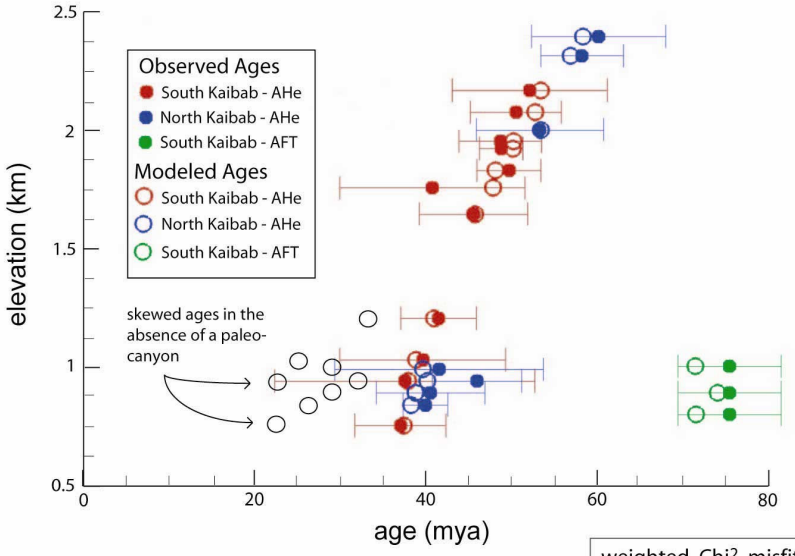

weighted Chi^2 misfit - 0.24

B. Best fit erosion history and subsequent unroofing

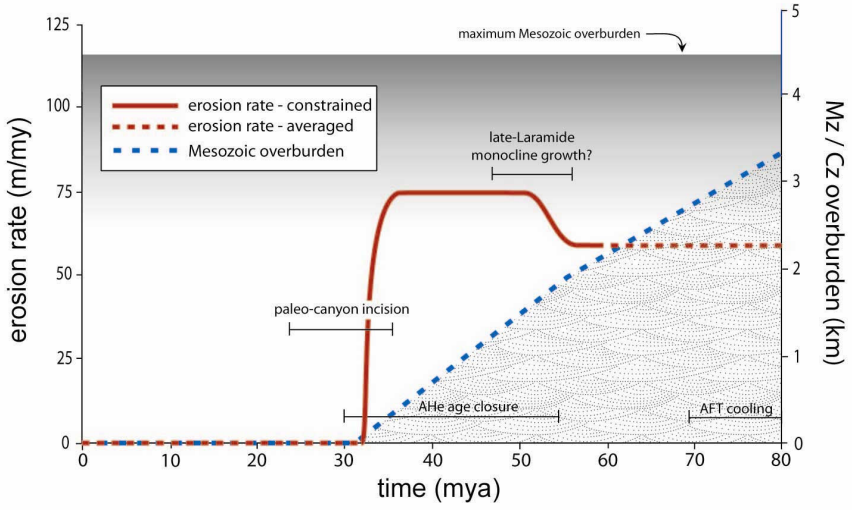

This Page Intentionally Left Blank

CHAPTER 2: Cenozoic Unroofing of the Grand Canyon Region

Chapter Summary

Drainage evolution and erosion patterns of the uplifted Colorado Plateau have eluded accurate description for over century. Early scientific expeditions in the region questioned the Colorado River's unlikely course against structural grain and through structural highs. Recent denudation of the region, largely driven by recent drainage integration of the Colorado River, has resulted in a relative lack of Cenozoic rock record and complicated the assessment of landscape and drainage evolution in response to driving tectonics forces. This study employs low-temperature thermochronology to quantify cooling patterns in response to erosional unroofing in the Grand Canyon region. New apatite (U-Th)/He (AHe) and fission track (AFT) sample datasets consist of four vertical transects, four boreholes, and a lateral transect along the Colorado River. Ages span from late-Cretaceous to Miocene and are believed to correspond to laterally variable erosion patterns throughout the region. Inverse modeling of viable thermal histories is used to establish representative closure temperatures for both AFT and AHE. The calculation of overburden thickness is then calculated at the time of age closure assuming a geothermal gradient and surface temperature. Extrapolation of these unroofing patterns to time slices then allows the construction of time stepped unroofing profiles. The results provide the highest resolution unroofing schedule for the Grand Canyon to date and indicate the following events: (1) early-Laramide planation and Eocene formation of the Kaibab Uplift, (2) Significant post-Laramide erosion, and (3) late Miocene unroofing almost 2 km of overburden from the Lee's Ferry region.

I. Introduction

The origin and evolution of the upper Colorado River system on the Colorado Plateau region has puzzled scientists, since early scientific expeditions to the Grand Canyon over a century ago (e.g., Dutton, 1882; Hunt, 1956). The long-term Cenozoic evolution of the river system in response to tectonic events, such as Sevier and Laramide contraction or Basin and Range extension and the development of the modern, deeply incised Colorado River in the Grand Canyon region of the Colorado Plateau have raised many questions (Hunt, 1956; McKee et al., 1967; Hunt, 1969). In particular, the Neogene evolution of the Colorado River in the Grand Canyon has remained enigmatic, since the river flows against the regional structural and topographic grain as it carves through Laramide monoclines (Young and Brennan, 1974; Young and McKee, 1978). In addition, a poorly understood Cenozoic flow reversal of the Colorado River and delayed plateau-wide drainage integration further complicate drainage development (Young and McKee, 1978). Since drainage evolution and landscape development are closely linked on the Colorado Plateau, quantitative description of the style, timing, and magnitude of erosion and removal of Mesozoic (>2 km) and Paleozoic strata that covered much of the Grand Canyon is critical for a better understanding of the Cenozoic evolution of the upper Colorado River system. Reconstruction of the long-term erosional landscape evolution is hampered by sparse geologic evidence from the Mesozoic and Cenozoic rock record. Recent developments in low-temperature thermochronometry, however, make it possible to constrain due to new analytical techniques in combination with a better quantitative understanding how topographic cooling during erosion and incision

influence closure isotherm geometries landscape evolution and erosion patterns through time (Braun, 2002, 2005; Ehlers, 2005). The potential and strength of this approach in assessing paleo-topographic environments and unroofing patterns has been documented in several studies (House et al., 1997; Brown et al., 2002; Ehlers and Farley, 2003; Ehlers et al., 2006). This study presents new low-temperature thermochronometric data from the Grand Canyon region and provides new constraints on the erosional history and landscape evolution of the Colorado Plateau in the vicinity of the Grand Canyon through a combination of apatite fission track (AFT) and (U-Th)/He (AHe) thermochronometry on surface and borehole samples and thermal modeling. Substantial topographic relief (>1.5km) and laterally continuous stratigraphy and hence thermophysical properties make the Grand Canyon region an excellent candidate for applying thermochronometric techniques in an attempt to answer ambiguities regarding drainage and landscape evolution.

2. Background and Approach

2.1 Geologic Setting

2.1.1 The Colorado Plateau

The Colorado Plateau represents an unusual geologic and tectonic province of the western United States that lacks significant Cenozoic structural deformation despite being surrounded by the highly extended domains of the Basin and Rang and the Rio Grande rift. Despite the relatively undeformed nature, it averages an elevation of ~1900 m (Pederson et al., 2002b) and has undergone significant surface and rock uplift as well as erosional denudation and fluvial incision since the latest Cretaceous. A number of

models have been proposed to explain how the plateau came to stand at a modern elevation with only minor reactivation of basement structures and the temporal and causal relationship between surface uplift and rock uplift and exhumation of the Colorado Plateau (e.g., Spencer, 1996; McQuarrie and Chase, 2000; Roy et al., 2004b). These models include different mechanisms ranging from early to middle Cenozoic Laramide deformation to middle to late Cenozoic epeirogeny and steam incision.

The geology of the Grand Canyon region (Fig. 1) exposes rocks recording the Proterozoic growth of North America and rich depositional history of the long-lived Phanerozoic passive continental margin (ch 6-12, McKee, 1974; Beus and Morales, 2003b); a rock record that has attracted geologists and tourist alike for well over a century. The little deformed Paleozoic section, exposing predominantly Cambrian to Permian sandstone and limestone, measures over one kilometer in thickness in the Grand Canyon region (Beus, 1990; Middleton, 1990), while Mesozoic strata is now largely absent on the southwestern Colorado Plateau. The Mesozoic sedimentary section once extended over the Grand Canyon region and is still preserved in the region north of the canyon, where it reaches thicknesses of up to 2.5-3.5 km in the Books Cliffs/Canyonlands region (Hintze, 1988; Billingsley, 1989). Although no direct evidence has constrained the thickness of the Mesozoic section once present over the Grand Canyon, thermochronometric studies have suggested the presence of ~3-4 km of Mesozoic overburden near the end-Cretaceous (Dumitru et al., 1994; Kelley et al., 2000; Flowers et al., 2007).

2.1.2 Mesozoic and Cenozoic Structural Overview

Tectonic provinces of intense structural deformation border the modern Colorado Plateau on all sides: the Rocky Mountains to the northeast, Uinta Uplift to the north, Basin and Range to the west and southwest and the Rio Grand Rift to the southeast. The Colorado Plateau, however, has experienced relatively little deformation throughout the Phanerozoic. The most intense Phanerozoic deformation occurred in the late-Cretaceous to Eocene thick-skinned contractional deformation resulting in the formation of uplifts due to minor reactivation of basement structures (e.g., Morgan and Swanberg, 1985). These uplifts have the appearance of large, doubly plunging, asymmetrical anticlines that are characterized by gently dipping backlimbs and a narrow, moderately to steeply dipping forelimbs in the form of a monocline and can be regarded as fault propagation folds (Tindall and Davis, 1999). In the case of the Kaibab uplift, in the Grand Canyon region, the monocline can be seen to root in a steeply dipping Precambrian fault (Davis, 1978; Huntoon, 1993) which upon reactivation in the Laramide drove fault-propagation folding along the East Kaibab monocline (Fig. 1). Timing of monocline formation in the Grand Canyon region has been difficult to constrain, but has been suggested to be late late-Laramide (Eocene) (Young, 1979). Despite relatively minor upper-crustal deformation, the formation of Laramide uplift has been suggested to trigger the removal of over 310,000 km³ of Phanerozoic strata from the southwestern Colorado Plateau (Potochnik, 2000; Flowers et al., 2008) and incision of canyons >1 km in depth along the southwestern margin of the Colorado Plateau (Peirce et al., 1979; Lucchitta, 1984). These canyons contain coarse-clastic strata derived from the Sevier highlands directly to the west and Mogollon highlands to the south (Potochnik, 2000; Young, 2000).

Middle to late Cenozoic extensional faulting, associated with formation of the Basin and Range province, is expressed in the Grand Canyon region in the form of three significant normal fault systems: the Hurricane, Toroweap, Grand Wash Faults, and other faults of the Basin and Range transition zone (Davis, 1978; Huntoon, 1993). Initiation age and magnitude of normal slip on the Hurricane and Toroweap faults are not well-constrained but are thought to have initiated by ~3.5 Ma and ~2 Ma (Billingsley, 2000). Motion along the Grand Wash Fault is thought to have initiated as early as ~18 Ma (Young and Brennan, 1974; Lucchitta, 1979) and is only slightly older than inception of large-magnitude middle Miocene extension in the adjacent Gold Butte and Virgin River blocks (Fitzgerald et al., 1991). Measurable downwarping of ~1° of the southwestern Colorado Plateau has been attributed to middle-Cenozoic extension (Elston and Young, 1989). The modern topographic expression of the Basin and Range transition zone is thought to have been largely present by 13 Ma along the southwestern margin of the Colorado Plateau (Faulds et al., 2000a).

2.1.3 Drainage System Evolution

A sparse late Cenozoic rock record on the Colorado Plateau hampers detailed reconstruction of the proto-Colorado River drainage system and only allows limited insights. One of the most important observations illustrating fundamental changes in long-term drainage organization pertains to the paleo-flow directions. While the modern Colorado River flows westward across the southwestern margin of the Colorado Plateau, paleo-current direction indicators in gravels, filling early-Cenozoic paleo-canyons, suggest a regional east-flowing drainage system (Potochnik, 2000; Young, 2000). These

so-called “rim gravels” (Peirce et al., 1979; Peirce and Nations, 1986) contain Precambrian basement clasts shed from eroding, high-standing source terrains to the west and south that further support the presence of a north-east directed drainage system during the early Cenozoic (Bilodeau, 1986; Burchfiel et al., 1992). Formation of the basement-cored monoclines on the Colorado Plateau during Laramide thick-skinned thrusting are thought to have forced continuous adjustments to the drainage system as the uplifts likely leading to compartmentalization and disruption of local drainage patterns (Huntoon, 2003).

The exact timing of Neogene drainage reversal of the proto-Colorado River drainage system is not well constrained, but there is consensus that the present western Grand Canyon took its shape only in the last 5.5 Ma (Lucchitta and Jeanne Richard, 2000; Lucchitta, 2003). It has been documented that the western Grand Canyon took its shape after emplacement of the late Miocene Shivwits basalt (Lucchitta and Jeanne Richard, 2000) and after deposition of the ~6 Ma Muddy Creek Formation and Hualapai Limestone (Castor and Faulds, 2000; Faulds et al., 2000b; Spencer et al., 2000). Incision of the western Grand Canyon began <6 Ma as a result of the integration of drainages from the elevated Colorado Plateau, through basins in the Basin and Range province, to a lowered base level in the Gulf of California that had been opening since the latest Miocene (McDougall et al., 1999; Oskin and Stock, 2003). Sediments from the Colorado Plateau first reached the Gulf at ~5.4 Ma (Dorsey et al., 2005) suggesting that the Colorado River system had achieved its modern course.

2.1.4 Scientific Rationale and Unresolved Questions

As previously outlined, the lack of a rich Mesozoic and Cenozoic sedimentary rock record in the area of the Grand Canyon complicates the reconstruction of the drainage evolution of the Colorado River and the erosional denudation of the southwestern Colorado Plateau. However, description of the drainage evolution and incision of the Grand Canyon is undoubtedly related to resolving the region's Cenozoic landscape evolution. Specifically, what is the style, timing, and magnitude of erosional denudation and removal of the Mesozoic overburden from the southwestern Colorado Plateau? Additionally, did middle-Cenozoic landscape evolution allow the presence of a through-flowing drainage system, or did the Laramide features compartmentalize and segment drainage system late into the Cenozoic? Despite recent thermochronometric studies, providing a broad description of the early-Laramide beveling and subsequent removal of Mesozoic overburden from the southwestern Colorado (Dumitru et al., 1994; Flowers et al., 2008) a more detailed and comprehensive landscape evolution reconstruction, derived from high-density thermochronometry, is required to better and more fully understand the evolution of the Colorado River drainage system.

2.2 Methodology

2.2.1 Apatite (U-Th)/He and Fission Track Thermochronology

(U-Th)/He dating of apatite is now a well-established thermochronological technique and is widely applied in geological, tectonic, and geomorphologic studies (e.g., Farley, 2000; Stockli et al., 2000; Farley and Stockli, 2002; Ehlers and Farley, 2003). (U-Th)/He dating of apatite is based on the radiogenic production of He from the alpha

decay of ^{235}U, ^{238}U, and ^{232}Th. The high-energy alpha decay results in emission of the α particle, leading to potential α loss from the grain during decay (Farley et al., 1996). This effect is routinely corrected using a statistical approach taking into account the alpha stopping distance, grain geometry, and mineral density (Farley et al., 1996). Radiogenic He is completely expelled from apatite at temperatures above ~80°C and almost totally retained below ~40°C (termed the He Partial Retention Zone, HePRZ) (Wolf et al., 1998; Stockli et al., 2000). Assuming a mean annual surface temperature of 10±5° C and a geothermal gradient of 25°C/km, the relevant temperature range is equivalent to depths of ~1 to 3 km. As an additional complication, Shuster and others (2006) demonstrated that radiation damage affect He diffusion kinetics in apatite, leading to an increased retentivity and thus increasing the effective closure temperature. This effect is most pronounced for apatite with elevated effective U concentrations that undergo protracted cooling histories, residing for substantial times between <150°C (annealing temperature of radiation damage).

Fission-track dating of apatite is based on the decay of trace ^{238}U by spontaneous nuclear fission (e.g., Fleischer et al., 1975; Dumitru, 2000; Gleadow et al., 2002). The use of apatite fission-track methods for thermochronometric analysis depends on the fact that tracks are partially or entirely annealed (erased) by thermally induced recrystallization at elevated subsurface temperatures, causing reductions in both the lengths of individual tracks and the fission-track ages. Temperature and chemical composition appear to be the predominant factors controlling fission-track annealing in apatite. The quantitative understanding of fission track annealing kinetics allow partially annealed apatite fission track apparent ages and confined length data to be used to

constrain the thermal evolution (~60-110° C) of samples using stochastic inverse modeling approaches (e.g., Gallagher, 1995; Ketcham, 2005). In this study, thermal histories were extracted from apatite fission track age and track-length populations and apatite (U-Th)/He ages using HeFTy modeling software (Ketcham, 2005).

2.2.2 Overburden Calculation

Unroofing patterns can be resolved through thermochronometric estimation of overburden thickness (OB_t) through time (Fig. 2). Free parameters in depth calculations are the geothermal gradient (G_o=25°C/km), surface temperature (T_s=10°C), and closure temperature (T_c). Because closure temperature is often a function of thermal history, the assignment of closure temperatures was accomplished by the inverse modeling of AHe and AFT age pairs (see the following section, 2.2.3, for a more in-depth explanation of this procedure). Closure temperatures can then be extracted from the output thermal history windows by examining the viable temperature variability at the time of each sample age closure (i.e. sample age). Representative closure temperatures were found to be 50°C for AHe and 90°C for AFT. These values are in agreement with closure temperatures theoretically calculated for variable cooling rates and grain sizes by (Reiners, 2005). (U-Th)/He and FT ages roughly correspond to total overburden thicknesses (OB_t) of 1.6 km and 3.2 where $OB_t = (T_c - T_s)/G_o$ (see appendix C for the calculation spreadsheet).

To avoid elevation related complications due to the effects of regional and local uplift and subsidence, absolute sample elevations (Es) are converted to a Kaibab normalized depth (KND, see Fig. 2). In this way, all elevations and the subsequent

overburden thicknesses, are normalized to a stratigraphic reference plane that was once extensive and roughly horizontal in the late Permian during passive continental margin deposition, the uppermost Kaibab Limestone surface (Hopkins and Thompson, 2003). This technique allows the calculation of overburden thickness independent of subsequent uplift and structural deformation as well as variation in each sample's stratigraphic position and has been employed in other recent thermochronologic studies in the region (Flowers et al., 2008). Calculation of the KND requires an elevation of the Kaibab surface (E_k) directly above the sample location. However, the modern Kaibab erosion surface is absent above many samples and the surface is non-horizontal. In these cases, Kaibab elevations are calculated by projecting a linear surface across the canyon and then projecting the sample's position vertically (see appendix D). Sample elevation is then subtracted from the Kaibab elevation (E_k).

2.2.3 Thermal History Modeling

Inverse thermal modeling, as mentioned in the previous section, was employed to calculate representative closure temperatures and identify possible cooling histories for samples yielding multiple thermochronologic ages. These thermal histories were calculated by an software package called HeFTy (Ketcham, 2005) (see Fig. 3). Apatite (U-Th)/He and fission track data (e.g. track lengths, number of tracks, grain diameter, diffusion parameters, [U], [Th], [Sm], etc.) are input as well as user defined constraints on the thermal history. Forward modeling of thousands of thermal histories randomly selected within the user defined constraints are used to calculate AFT and AHe ages. Calculated ages that lie within error of observed ages and track length distributions are

then considered viable thermal histories. The red thermal history paths in figure 3 represent these viable continuous thermal histories that theoretically produce the observed ages. Although these modeled thermal histories are not directly used to calculate overburden removal, they do agree with the results from overburden calculation methods outlined in section 2.2.2.

3. Thermochronometric Data

3.1 Sample Description and Age Data

Sample collection for this study was in such a fashion as to optimize the assessment of three-dimensional unroofing patterns (Fig. 1). Other thermochonologic studies have shown the vertical erosion schedule and style in the eastern Grand Canyon (this study, chapter 1). This study provides evidence for a lateral unroofing history along course of the Grand Canyon and on Coconino Plateau to the south of the Grand Canyon. Sample collection is comprised of 4 vertical transects, 4 boreholes, and a near-horizontal transect (previously collected and discussed by Kelley et al., 2000).

3.1.1 Vertical Transects

Vertical Transects were collected from the North and South Kaibab trails and the Bill Hall/Thunder River trails from the eastern Grand Canyon, and from Saddle Horse Canyon, near Toroweap Overlook in the central Grand Canyon. The North and South Kaibab transects span the Grand Canyon from rim to rim across the axis of the Kaibab Uplift. The South Kaibab transect produced 14 ages from 16 samples and spanned a vertical 1.40 km. AHe ages, shown in figure 4, ranged from 51.8 my at the south rim to

36.8 my at the Colorado River and yielded a highly linear age/elevation trend. The North Kaibab transect yielded 7 ages from 13 samples over an elevation differential of 1.63 km. AHe ages ranged from 59.8 Ma at the North Rim to 39.7 Ma near the Colorado River.

The Bill Hall/Thunder River trails provided an additional transect on the western flank of the Kaibab Uplift. These samples yielded a total of 5 AHe ages from 9 samples that ranged from 58.3 on the North Rim to 32.6 near the Colorado River and spanned a 1.48 km elevation differential. AHE ages from the North Kaibab, South Kaibab, and Bill Hall/Thunder River transects largely lie within error of an average age/elevation trend. Three outliers are identified in the South Kaibab dataset due to the disagreement in age from samples in close proximity and are thought to be the result of undetected U and Th rich inclusions.

A final vertical transect was collected from the Saddle Horse Canyon near the Toroweap overlook area, but yielded highly scatted, unreliable results. Insufficient apatite in the rock samples resulted in limited analytical analysis. Additionally, a complicated thermal structure due to local Cenozoic volcanism and insufficient maximum burial temperatures due to decreasing Mesozoic thickness towards the west are thought to have aided in AHe age scatter.

3.1.2 Boreholes

Borehole samples consisted of slices from 2 to 4 inch solid core and core chips provided by the USGS core research facility in Denver, CO. All boreholes were drilled from the Coconino plateau, to the south of the Grand Canyon. Borehole samples generally yielded highly scattered ages (Fig. 5, Tbl. 1). The lack of age reproducibility

was the result of the small sample sizes available from the 2 to 4 inch drill cores and the limited lithologic selection. The Blue Mountain core produced the shallowest samples and AHe ages ranged from 66.8 ± 9.2 Ma for the shallowest sample to 78.0 ± 10.2 Ma for the middle sample. Partial helium loss, as a result of elevated surface temperatures in the Miocene under the Blue Mountain basalt flow, are thought to have contributed to the age inversion of the shallowest sample. SBF samples represent a composite core (from SBF-9 and SBF-10) and produced five AHe ages ranging from 127 ± 18.2 Ma to 47.4 ± 9.4. The Sage Breccia Pipe samples produced only two AHe ages: 76.9 ± 9.9 Ma and 67.9 ± 28.0 Ma at depths of 206 m and 393 m respectively.

Relatively reproducible ages were produced from the Wate 1 dill core due to favorable lithology. These ages range from 47.7 ± 11.8 to 39.0 ± 7.8 Ma and result in a linear age/elevation trend. These samples ages also lie in close approximation to the observed ages for elevation equivalent samples from the North Kaibab, South Kaibab, and Thunder River vertical transects (see Fig. 4).

3.1.3 Lateral Transect

An additional dataset was collected from samples that form a lateral transect along the course of the Grand Canyon near the level of the Colorado River from Lee's Ferry, Arizona to Quartermaster Canyon in the western Grand Canyon (see Fig. 1). Initially collected for fission track analysis and published (Kelley et al., 2000), the sample separates have been reanalyzed for apatite (U-Th)/He ages. A total of 13 samples provided enough quality apatite for both apatite fission track (AFT) and apatite (U-Th)/He (AHe) analysis (Fig. 6, Tbl. 2). AFT ages range from 74±9 Ma on the western

side of the reactivated Toroweap fault to 28±3 Ma at Lee's Ferry. Ages exhibit a roughly linear average trend with increasing ages towards the west (see Fig. 6). A large (28±13 Ma) age jump occurs across the reactivated Toroweap Fault with the older ages on the western (currently downthrown) block. This age discrepancy across the Toroweap fault is largely a result of post-cooling structural offset. AHe ages range from 83±8 Ma in the far western Grand Canyon to 11±6 Ma at Lee's Ferry. Unlike AFT ages, AHe ages show variance around the Kaibab Uplift with older ages along its axis and younger ages on the flanks. AFT/AHe age inversion occurs in the westernmost 2 samples (see section 4.1)

4. Results

4.1 Western Grand Canyon

Lateral transect samples from the western Grand Canyon (i.e. GC-89, -87, -86, -128, -34) yield and average AFT age of 57.7 ± 7.9 Ma and an average AHe age of 48.9 ± 8.4 Ma. Samples GC-128 and -34 lie in the hanging wall and foot wall, respectively, of the Toroweap fault at river miles 191 and 190. Post cooling structural offset of the samples results in a 27.8 m.y. and 13.2 m.y. AFT and AHe age gap between nearly adjacent samples. However, when utilizing stratigraphic depth rather than absolute elevation to calculate overburden thickness through time, the presence of significant reverse offset on the Toroweap Monocline is unnecessary to explain the observed age differential across the fault. Overburden calculations for GC-128 and -34 indicate near exposure of the modern Kaibab Limestone surface by 30 Ma. Due to age inversion of the westernmost samples, overburden thicknesses were not calculated for samples GC-89, -87, and -86.

Age inversion of these westernmost samples is difficult to address. Recent studies quantifying the effect of alpha radiation damage on diffusion mechanics have shown that increasing degrees of radiation damage lead to increased helium retentively (Shuster et al., 2006). This effect has been observed in samples collected in the Grand Canyon region (Flowers et al., 2007). However, annealing kinetics of the radiation damage is still largely unknown. It is possible that these samples were buried deep enough to partially anneal fission tracks, but not deep enough to eliminate radiation damage helium traps, leading to higher helium retentively and older calculated AHe ages. This effect is only seen in samples in the far-western Grand Canyon, as expected, because late-Cenozoic uplift of the southwestern Colorado Plateau led to a decreased thickness of overburden and lower maximum burial temperatures on the plateau boundary (see also Flowers et al, 2008).

4.2 Eastern Grand Canyon

Samples from the Eastern Grand Canyon (i.e. GC-123, -122, -20, -16, -11, -103) produce an average AFT age of 53.6 ± 6.6 Ma and an average AHe age of 30.2 ± 6.8 Ma. Stratigraphic depths (KND) are greatest atop the Kaibab Uplift (GC-11) and decrease on its flanks. For this reason, age closure corresponds to Mesozoic overburden thicknesses of 1.9-1.6 km for AFT and 0.3-0.0 km for AHe. The sample ages spanning the Kaibab Uplift also show a structural elevation/age correlation, with increased ages atop the uplift. This pattern is particularly evident in the AHe dataset. Calculated erosion rates of ~80 m/my, from ~60-30 Ma and along the axis of the Kaibab Uplift (samples GC-20, 16, 11), are in agreement with previous thermochronologic results (this study, chapter 1).

Continuous thermal histories, calculated by HeFTy, also independently suggest compatible erosion rates through the middle Cenozoic and also suggest a significant Miocene cooling event.

4.3 Lee's Ferry

Sample ages from Lee's Ferry averaged 29.2 ± 2.7 Ma (AFT) and 12.9 ± 3.6 Ma (AHe). Due to the relatively shallow stratigraphic depth of these samples the calculated Mesozoic overburden thicknesses were greater other samples. These samples indicate late Cenozoic unroofing of the area, with over 3 km of mesozoic overburden present at 30 Ma and almost 1.5 kilometers as late as 15 Ma. Continuous thermal histories also indicate elevated temperatures until 30 Ma, followed by relatively rapid unroofing.

4.4 Discussion

4.4.1 Laramide Erosion

Early Cenozoic AFT ages west of the Kaibab Uplift indicate a regional unroofing event that temporally corresponds with the Laramide orogeny. Previous works (i.e., Young, 1979, 2001; Flowers et al., 2008) on the southwest Colorado Plateau rim have also indicated regional denudation in response to broad flexure of the plateau rim in the latest Cretaceous. The structural elevation/age correlation present on the Kaibab Uplift also indicates that Eocene-to-Oligocene cooling patterns were influenced by low-relief planation of the Kaibab Uplift.

Laramide planation has also been suggested by independent treatment of thermochronologic vertical transects (this study, chapter 1). Additional supporting

evidence for the presence of Laramide low-relief denudation is provided by the consideration of all vertical datasets. Figure 4 illustrates a regional cooling pattern that is common to all samples collected near (i.e. vertical transects) and far (Wate borehole) from the modern canyon. This study (chapter 1) shows that the borehole samples are far enough removed to experience no significant topographically induced cooling influence from a paleo-canyon, had there been such a canyon. The agreement of ages between borehole and vertical transect data infers an age/elevation invariance; a diagnostic property of cooling in a horizontal isotherm regime (this study, chapter 1).

4.4.2 Post-Laramide Erosion

Widespread exposure of the Kaibab Limestone surface west of the Kaibab Uplift did not occur until ~30-35 Ma, indicating significant erosion in a post-Laramide environment. It is unclear if this Oligocene erosion episode is a result of delayed erosion due to protracted drainage integration if one must invoke a middle-Cenozoic uplift event to fuel the post-Laramide erosion. Relatively younger AHe ages are observed on the flanks of the Kaibab Uplift, indicate gradual retreat of the Mesozoic/Cenozoic strata from the axis of the Kaibab Uplift. The presence of Mesozoic strata in the areas adjacent to the Kaibab Uplift also indicates that a regionally low-relief environment could have persisted west of the Kaibab Uplift despite the structural relief. It has also been shown (this study, chapter 1) that exposure of the Kaibab surface on the Kaibab Uplift was soon followed by localized incision and creation of a paleotopographic canyon. Partial deflection of the Colorado River's course at the Kaibab Uplift might also support this idea, where the

modern course of the river may indicate the Permian/Triassic stratigraphic interface at the time of incision.

Finally, the presence of over ~2.5 km of Mesozoic overburden near Lee's Ferry in the early Miocene indicates that, in the absence of additional structural complexity, the Lee's Ferry area was topographically higher than the adjacent Kaibab Uplift, possibly in excess of 1km at ~15 Ma. The presence of such paleorelief would have certainly had an impact on the local drainage system by inhibiting eastward flow.

5. Conclusions

The unroofing history outlined in this study offers a new level of detail in the description of landscape evolution for the Grand Canyon region. The contrasting unroofing histories of Lee's Ferry, the Kaibab Uplift and the western Grand Canyon reveal the lateral variability in erosion patterns through time. Furthermore, these erosion patterns contrast with those of the central Colorado Plateau. Previous and ongoing work on the unroofing of the Colorado Plateau in general, suggests a large degree of regional variability in such erosion histories. This study helps to punctuate this pattern. For this reason, uplift mechanisms for the Colorado Plateau, which may be spatially variable themselves, must consider this complicated and irregular erosion history.

Ongoing work related to this study will continue to further resolve the landscape evolution of the Grand Canyon region. Additional river level samples are currently being analyzed to supplement the existing lateral transect ages as will incorporation of previously published additional AFT data (Kelley et al., 2000). Finally, unroofing

profiles based upon the continuous thermal histories produced by inverse modeling techniques will provide a high resolution, temporally continuous, unroofing history.

REFERENCES CITED

Beus, S. S., 1990, Temple Butte Formation.; Grand Canyon Geology, p. 107-118.

Beus, S. S., and Morales, M., 2003, Grand Canyon Geology, Oxford University Press, 432 p.

Billingsley, G. H., 1989, Mesozoic strata at Lees Ferry, Arizona.; Geology of Grand Canyon, northern Arizona (with Colorado River guides); Lees Ferry to Pierce Ferry, Arizona.; Field trips for the 28th international geological congress. 1989, p. 137-138.

-, 2000, Volvanic events of the past 20 Ma in the western Grand Canyon region, Significance to Grand Canyon region, *in* Young, R. A., ed., Abstracts for a working conference on the Cenozoic geological evolution of the Colorado River system and the erosional chronology of the Grand Canyon region: Grand Canyon, Arizona, Grand Canyon Association, p. 1-3.

Bilodeau, W. L., 1986, The Mesozoic Mogollon Highlands, Arizona; an Early Cretaceous rift shoulder: Journal of Geology, v. 94, no. 5, p. 724-735.

Braun, J., 2002, Quantifying the effect of Recent relief changes on age-elevation relationships: Earth and Planetary Science Letters, v. 200, no. 3-4, p. 331-343.

-, 2005, Quantitative constraints on the rate of landform evolution derived from low-temperature thermochronology.; Low-temperature thermochronology; techniques, interpretations, and applications: Reviews in Mineralogy and Geochemistry, v. 58, no. 1, p. 351-374.

Brown, R. W., Cockburn, H. A. P., Kohn, B. P., Belton, D. X., Fink, D., Gleadow, A. J. W., and Summerfield, M. A., 2002, Combining low temperature apatite thermochronology and cosmogenic isotope analysis in quantitative landscape evolution studies.; Abstracts of the 12th annual V. M. Goldschmidt conference: Geochimica et Cosmochimica Acta, v. 66, no. 15A, p. 106.

Burchfiel, B. C., Cowan Darrel, S., and Davis Gregory, A., 1992, Tectonic overview of the Cordilleran Orogen in the Western United States.; The Cordilleran Orogen; conterminous U.S.; The geology of North America. 1992, p. 407-479.

Castor, S. B., and Faulds, J. E., 2000, Post-6 Ma limestone along the southeastern part of the Las Vegas Valley shear zone, southern Nevada.; Colorado River origin and evolution; proceedings of a symposium, p. 77-79.

Davis, G. H., 1978, Monocline fold pattern of the Colorado Plateau.; Laramide folding associated with basement block faulting in the western United States: Memoir Geological Society of America, p. 215-233.

Dorsey, R. J., Fluette, A., McDougall, K., Housen, B. A., and Janecke, S. U., 2005, Terminal Miocene arrival of Colorado River sand in the Salton Trough, Southern California; implications for initiation of the lower Colorado River drainage.; Geological Society of America, 2005 annual meeting: Abstracts with Programs Geological Society of America, v. 37, no. 7, p. 109.

Dumitru, T. A., Duddy, I. R., and Green, P. F., 1994, Mesozoic-Cenozoic burial, uplift, and erosion history of the west-central Colorado Plateau; with Suppl. Data 9428: Geology (Boulder), v. 22, no. 6, p. 499-502.

Ehlers, T. A., 2005, Crustal thermal processes and the interpretation of thermochronometer data.; Low-temperature thermochronology; techniques,

interpretations, and applications: Reviews in Mineralogy and Geochemistry, v. 58, no. 1, p. 315-350.
Ehlers, T. A., and Farley, K. A., 2003, Apatite (U-Th)/ He thermochronometry; methods and applications to problems in tectonic and surface processes: Earth and Planetary Science Letters, v. 206, no. 1-2, p. 1-14.
Ehlers, T. A., Farley, K. A., Rusmore, M. E., and Woodsworth, G. J., 2006, Apatite (U-Th)/ He signal of large-magnitude accelerated glacial erosion, southwest British Columbia: Geology (Boulder), v. 34, no. 9, p. 765-768.
Elston, D. P., and Young, R. A., 1989, Development of Cenozoic landscape of central and northern Arizona; cutting of Grand Canyon.; Geology of Grand Canyon, northern Arizona (with Colorado River guides); Lees Ferry to Pierce Ferry, Arizona.; Field trips for the 28th international geological congress. 1989, p. 145-153.
Farley, K. A., 2000, Helium diffusion from apatite; general behavior as illustrated by Durango fluorapatite: Journal of Geophysical Research, B, Solid Earth and Planets, v. 105, no. 2, p. 2903-2914.
Farley, K. A., and Stockli, D. F., 2002, (U-Th)/ He dating of phosphates; apatite, monazite, and xenotime.; Phosphates; geochemical, geobiological, and materials importance: Reviews in Mineralogy and Geochemistry, v. 48, p. 559-577.
Farley, K. A., Wolf, R. A., and Silver, L. T., 1996, The effects of long alpha-stopping distances on (U-Th)/He ages: Geochimica et Cosmochimica Acta, v. 60, no. 21, p. 4223-4229.
Faulds, J. E., Price, L. M., and Wallace, M. A., 2000a, Pre-Colorado River paleogeography and extension along the Colorado Plateau-Basin and Range boundary, northwestern Arizona.; Colorado River origin and evolution; proceedings of a symposium, p. 93-99.
Faulds, J. E., Wallace, M. A., Gonzales, L. A., and Heizler, M. T., 2000b, Depositional environment and paleogeographic implications of the late Miocene Hualapai Limestone, northwestern Arizona and southern Nevada.; Colorado River origin and evolution; proceedings of a symposium, p. 81-87.
Fitzgerald, P. G., Fryxell, J. E., and Wernicke Brian, P., 1991, Miocene crustal extension and uplift in southeastern Nevada; constraints from fission track analysis: Geology (Boulder), v. 19, no. 10, p. 1013-1016.
Flowers, R. M., Shuster, D. L., Wernicke, B. P., and Farley, K. A., 2007, Radiation damage control on apatite (U-Th)/ He dates from the Grand Canyon region, Colorado Plateau: Geology (Boulder), v. 35, no. 5, p. 447-450.
Flowers, R. M., Wernike, B., and Farley, K. A., 2008, Unroofing, Incision and Uplift History of the Southwestern Colorado Plateau from (U-Th)/He Apatite Thermochronometry: GSA Bulletin, in press.
Gallagher, K., 1995, Evolving temperature histories from apatite fission-track data: Earth and Planetary Science Letters, v. 136, no. 3-4, p. 421-435.
Hintze, L. F., 1988, The Geologic History of Utah: Geology Studies. Special Publication, v. 7.
Hopkins, R. L., and Thompson, K. L., 2003, Kaibab Formation.; 2.; Grand Canyon geology, p. 196-211.

House, M. A., Wernicke, B. P., Farley, K. A., and Dumitru, T. A., 1997, Cenozoic thermal evolution of the central Sierra Nevada, California, from (U-Th)/ He thermochronometry: Earth and Planetary Science Letters, v. 151, no. 3-4, p. 167-179.
Hunt, C. B., 1956, Cenozoic Geology of the. Colorado Plateau: U. S. Geological Survey Professional Paper.
-, 1969, Geologic history of the Colorado River.; The Colorado River region and John Wesley Powell: U, p. C59-C130.
Huntoon, P. W., 1993, Influence of inherited Precambrian basement structure on the localization and form of Laramide monoclines, Grand Canyon, Arizona.; Laramide basement deformation in the Rocky Mountain foreland of the Western United States: Special Paper Geological Society of America, v. 280, p. 243-256.
-, 2003, Post-Precambrian tectonism in the Grand Canyon region.; 2.; Grand Canyon geology, p. 222-259.
Kelley, S. A., Chapin, C. E., and Karlstrom, K. E., 2000, Laramide cooling histories of Grand Canyon, Arizona, and the Front Range, Colorado, determined from apatite fission-track thermochronology.; Colorado River origin and evolution; proceedings of a symposium, p. 37-41.
Ketcham, R. A., 2005, Forward and inverse modeling of low-temperature thermochronometry data.; Low-temperature thermochronology; techniques, interpretations, and applications: Reviews in Mineralogy and Geochemistry, v. 58, no. 1, p. 275-314.
Lucchitta, I., 1979, Late Cenozoic uplift of the southwestern Colorado Plateau and adjacent lower Colorado River region.; Plateau uplift; mode and mechanism: Tectonophysics, v. 61, no. 1-3, p. 63-95.
-, 1984, Development of landscape in northwestern Arizona; the country of plateaus and canyons.; Landscapes of Arizona; the geological story, p. 269-301.
-, 2003, History of the Grand Canyon and of the Colorado River in Arizona.; 2.; Grand Canyon geology, p. 260-274.
Lucchitta, I., and Jeanne Richard, A., 2000, Geomorphic features and processes of the Shivwits Plateau, Arizona, and their constraints on the age of western Grand Canyon.; Colorado River origin and evolution; proceedings of a symposium, p. 65-69.
McDougall, K. A., Poore, R. Z., and Matti, J. C., 1999, Age and paleoenvironment of the Imperial Formation near San Gorgonio Pass, Southern California: Journal of Foraminiferal Research, v. 29, no. 1, p. 4-25.
McKee, E. D., 1974, Paleozoic rocks of Grand Canyon.; Geology of the Grand Canyon, p. 42-64.
McKee, E. D., Wilson, R. F., Breed, W. J., and Breed, C. S., 1967, Evolution of the Colorado River in Arizona; a hypothesis developed at the Symposium on Cenozoic Geology of the Colorado Plateau in Arizona, August 1964: Museum of Northern Arizona Bulletin, v. 6, p. 67.
McQuarrie, N., and Chase, C., 2000, Raising the Colorado Plateau: Geology (Boulder), v. 28, no. 1, p. 91-94.
Middleton, L. T. E., D.K., 1990, Redwall Limestone and Surprise Canyon Formation.; Grand Canyon Geology, p. 119-146.

Morgan, P., and Swanberg, C. A., 1985, On the Cenozoic uplift and tectonic stability of the Colorado Plateau: Journal of Geodynamics, v. 3, no. 1-2, p. 39-63.
Oskin, M., and Stock, J., 2003, Pacific-North America plate motion and opening of the Upper Delfin Basin, northern Gulf of California, Mexico: Geological Society of America Bulletin, v. 115, no. 10, p. 1173-1190.
Pederson, J. L., Mackley, R. D., and Eddleman, J. L., 2002, Colorado Plateau uplift and erosion evaluated using GIS: GSA Today, v. 12, no. 8, p. 4-10.
Peirce, H. W., Damon, P. E., and Shafiqullah, M., 1979, An Oligocene (?) Colorado Plateau edge in Arizona.; Plateau uplift; mode and mechanism: Tectonophysics, v. 61, no. 1-3, p. 1-24.
Peirce, H. W., and Nations, J. D., 1986, Tectonic and paleogeographic significance of Tertiary rocks of the southern Colorado Plateau and transition zone.; Geology of central and northern Arizona; field trip guidebook, Geological Society of America, Rocky Mountain Section meeting, Flagstaff, Arizona, 1986, p. 111-124.
Potochnik, A. R., 2000, Paleogeomorphic evolution of the Salt River region; implications for Cretaceous-Laramide inheritance for ancestral Colorado River drainage.; Colorado River origin and evolution; proceedings of a symposium, p. 17-22.
Reiners, P. W., 2005, Zircon (U-Th)/ He thermochronometry.; Low-temperature thermochronology; techniques, interpretations, and applications: Reviews in Mineralogy and Geochemistry, v. 58, no. 1, p. 151-179.
Roy, M., Kelley, S., Pazzaglia Frank, J., Cather, S., and House Martha, A., 2004, Middle Tertiary buoyancy modification and its relationship to rock exhumation, cooling, and subsequent extension at the eastern margin of the Colorado Plateau: Geology (Boulder), v. 32, no. 10, p. 925-928.
Shuster, D. L., Flowers, R. M., and Farley, K. A., 2006, The influence of natural radiation damage on helium diffusion kinetics in apatite: Earth and Planetary Science Letters, v. 249, no. 3-4, p. 148-161.
Spencer, J. E., 1996, Uplift of the Colorado Plateau due to lithosphere attenuation during Laramide low-angle subduction: Journal of Geophysical Research, B, Solid Earth and Planets, v. 101, no. 6, p. 13,595-13,609.
Spencer, J. E., Peters, L., McIntosh, W. C., and Patchett, P. J., 2000, (super 40) Ar/ (super 39) Ar geochronology of the Hualapai Limestone and Bouse Formation and implications for the age of the lower Colorado River.; Colorado River origin and evolution; proceedings of a symposium, p. 89-91.
Stockli, D. F., Farley, K. A., Dumitru, T. A., and Anonymous, 2000, Intercalibration and integration of apatite (U-Th)/ He and fission track thermochronometers on an exhumed extensional fault block, White Mountains, eastern California, U.S.A.; Fission track 2000; 9th international conference on fission track dating and thermochronology: Abstracts Geological Society of Australia, v. 58, p. 305-307.
Tindall, S. E., and Davis, G. H., 1999, Monocline development by oblique-slip fault-propagation folding; the East Kaibab Monocline, Colorado Plateau, Utah: Journal of Structural Geology, v. 21, no. 10, p. 1303-1320.
Wolf, R. A., Farley, K. A., and Kass, D. M., 1998, Modeling of the temperature sensitivity of the apatite (U-Th)/ He thermochronometer: Chemical Geology, v. 148, no. 1-2, p. 105-114.

Young, R. A., 1979, Laramide deformation, erosion and plutonism along the southwestern margin of the Colorado Plateau.; Plateau uplift; mode and mechanism: Tectonophysics, v. 61, no. 1-3, p. 25-47.
-, 2000, The Laramide-Paleogene history of the western Grand Canyon region; setting the stage.; Colorado River origin and evolution; proceedings of a symposium, p. 7-15.
-, 2001, Geomorphic, structural, and stratigraphic evidence for Laramide Uplift of the southwestern Colorado Plateau margin in northwestern Arizona.; The geologic transition, high plateaus to Great Basin; a symposium and field guide; the Mackin volume: Guidebook Pacific Section, American Association of Petroleum Geologists, v. 78, p. 227-237.
Young, R. A., and Brennan, W. J., 1974, Peach Springs Tuff; Its Bearing on Structural Evolution of the Colorado Plateau and Development of Cenozoic Drainage in Mohave County, Arizona: Geological Society of America Bulletin, v. 85, no. 1, p. 83-90.
Young, R. A., and McKee, E. H., 1978, Early and middle Cenozoic drainage and erosion in West-central Arizona: Geological Society of America Bulletin, v. 89, no. 12, p. 1745-1750.

FIGURE LIST

Sample Name	Age [Ma]	± [Ma]	# of analysis	[eU] (ppm)	elevation (m)	depth (m)	rock unit
Vertical Transects							
GCSK 1	51.8	20.1	5	47	2164	-	Kaibab Fm
GCSK 2	50.2	10.5	4	43	2073	-	Toroweap Fm
GCSK 3	48.4	9.6	4	23	1951	-	Coconino ss
GCSK 4	48.5	6.7	7	44	1920	-	Coconino ss
GCSK 5	60.9	7.5	3	38	1902	-	Coconino ss
GCSK 6	49.4	8.3	5	66	1829	-	Esplanade ss
GCSK 7	40.5	21.3	4	54	1756	-	Supai Grp
GCSK 8	66.1	5.2	3	31	1682	-	Supai Grp
GCSK 9	45.3	14.1	5	43	1646	-	Supai Grp
GCSK 10	41.2	8.7	4	39	1207	-	Tapeats ss
GCSK 12	39.4	19.1	4	38	1033	-	Bass Fm
GCSK 13	37.3	15.1	2	14	944	-	Vishnu Schist
GCSK 15	60.6	11.3	9	25	818	-	Brahma Schist
GCSK 16	36.8	5.3	2	7	758	-	Vishnu Schist
GCNK 1	59.8	15.6	4	25	2391	-	Toroweap Lm
GCNK 2	57.9	10.8	5	47	2309	-	Coconino ss
GCNK 4	53.0	16.5	5	71	1999	-	Supai ss
GCNK 9	41.3	12.1	3	19	993	-	Vishnu Schist
GCNK 10	45.7	12.7	6	4	944	-	Rama Schist
GCNK 11	40.3	6.3	1	9	896	-	Vishnu Schist
GCNK 12	39.7	5.2	4	3	843	-	Vishnu Schist
GCTR1	35.6	6.0	1	100	776	-	Tapeats ss
GCTR2	32.6	9.7	4	31	703	-	Hakatai shale
GCTR4	51.2	6.2	4	112	944	-	Bright Angel
GCTR8	56.8	16.8	5	68	1957	-	Coconino ss
GCTR9	58.3	7.5	2	13	2181	-	Kaibab Fm
Core Samples							
Wate1030	47.7	11.8	4	22	1496	314	-
Wate1255	47.1	25.9	4	26	1427	383	-
Wate1450	44.2	4.1	5	66	1368	442	-
Wate1610	39.0	7.8	2	42	1319	491	-
Wate1810	44.8	19.1	5	53	1258	552	-
Blue Mountain 1	66.8	9.2	6	27	-	31	-
Blue Mountain 2	78.0	10.2	6	47	-	73	-
Blue Mountain 3	73.3	3.4	2	47	-	138	-
SBF2	127.7	18.2	6	234	-	265	-
SBF5	69.6	5.7	4	72	-	381	-
SBF6	74.6	29.0	3	42	-	488	-
SBF7	47.4	9.4	4	43	-	549	-
SBF8	93.4	29.8	5	34	-	573	-
Sage Breccia 1	76.9	9.9	4	57	-	206	-
Sage Breccia 6	67.9	28.0	2	59	-	393	-

Table 2.1 (U-Th-Sm)/He age data for all vertical transects and the Wate borehole.

	(U-Th)/He Data				Fisson Track Data					Sample Information		
Sample	Age [Ma]	± [Ma]	# of analysis	[eU] (ppm)	Central Age (Ma) (±1 S.E.)	± [Ma]	# of grains	Mean Track Length (µm) (± 1 S.E.)	# of tracks	river mile	elv (m)	Rock Type
GC90	10.6	3.0	4	48.6	30	2.4	20	12.7±1.2	13	0	957	Shinarump ss.
GC92	15.1	4.1	5	90.6	28.4	2.9	20	12.2±1.0	17	3.5	945	Toroweap ss.
GC103	36.4	-	1	6	49	4.1	20	12.7	47	66.5	841	Dox Sandstone
GC11	33.1	14.3	2	10.1	49.4	3.8	20	11.1 ± 1.0	31	81.1	768	Vishnu Schist
GC16	37.9	7.1	4	11.0	59.9	5.8	20	11.4 ± 2.3	9	91.2	731	Trinity Gneiss
GC20	26.5	4.2	5	9	46.5	4.9	20	11.7 ± 0.8	49	96.1	720	Boucher Granite
GC122	29.0	-	1	3	58.6	12.2	18	-	-	116.6	701	granite
GC123	18.2	3.5	7	5.4	57.9	9	20	-	10	133.6	610	diabase
GC34	14.4	3.3	2	9.6	45.7	4.1	20	13.3 ± 0.8	14	190	488	Granitic gneiss
GC128	27.6	1.1	3	8.3	73.5	8.9	20	-	12	191	485	granite
GC86	50	21.6	3	14	62.8	4	20	13.0±0.4	67	240	372	granodiorite
GC87	82.5	7.5	7	152	55.9	3.2	20	12.1±0.4	101	252.5	366	granodiorite
GC89	69.8	8.7	3	24	50.4	19.2	3	-	-	265	366	granite

Table 2.2 Apatite fission track and (U-Th)/He data collected for the lateral transect.

Figure 2.1. A colored-relief map of the Grand Canyon region generated from a SRTM 90m digital elevation model. Included are sample locations, major structural and landscape features and faults, and a regional location inset.

The Grand Canyon, AZ

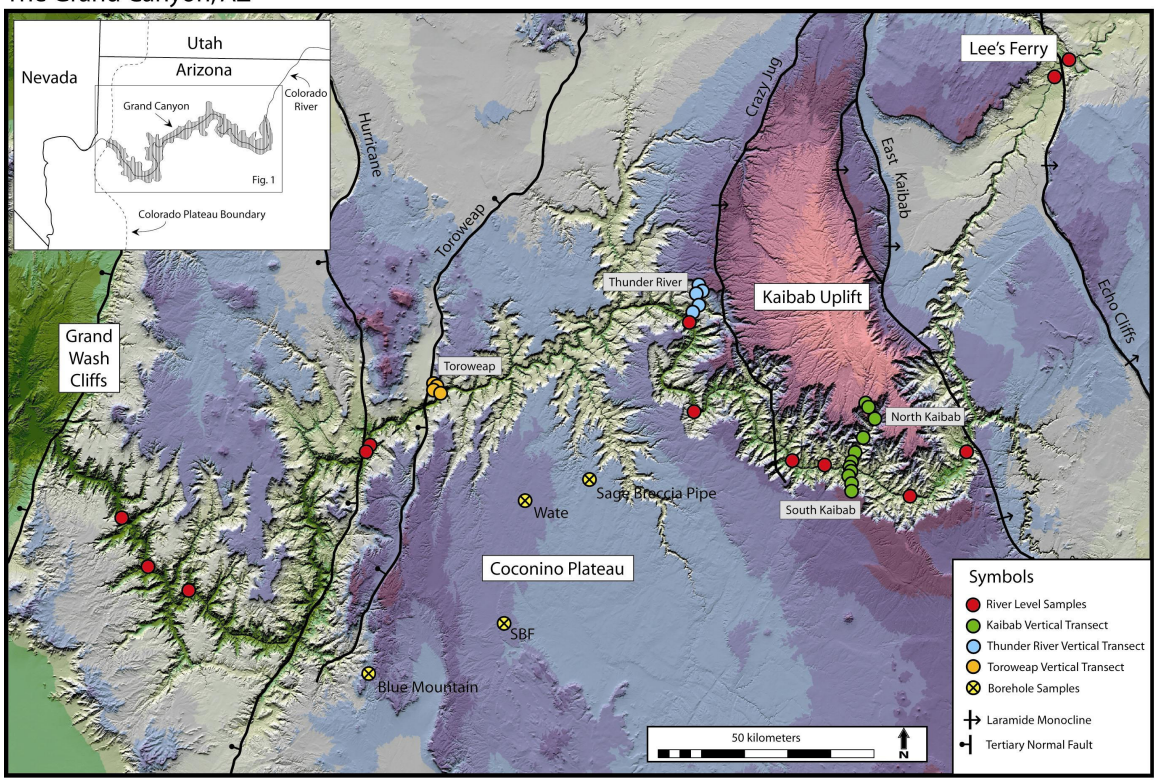

Figure 2.2. A diagrammatic illustration of the terminology used to calculate overburden thickness (also see table 2). Sample location is denoted by 'X'. Observed parameters include: Sample elevation (E_s), Kaibab elevation (E_k), surface temperature (T_s), geothermal gradient (G_o), and sample closure temperature (T_c). Calculated parameters include KND, Mesozoic overburden thickness (OB_{mz}), and total overburden thickness (OB_t): $KND = E_k - E_s$; $OB_t = (T_c - T_s)/G_o$; $OB_{mz} = OB_t - KND$.

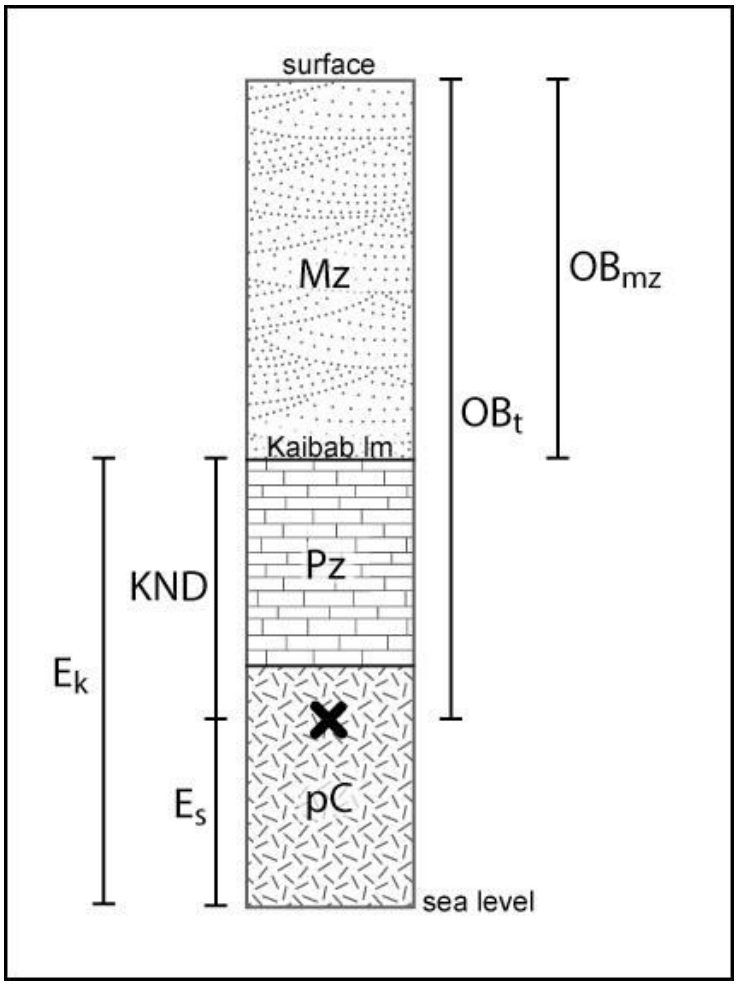
surface
Mz
OB$_{mz}$
OB$_t$
Kaibab lm
Pz
KND
E$_k$
E$_s$
pC
sea level

Figure 2.3. A thermal history profile generated by the HeFTy modeling package. Inputs include fission track and (U-Th)/He data included in Table 1. Modeled results agree with the results calculated in Table 2.

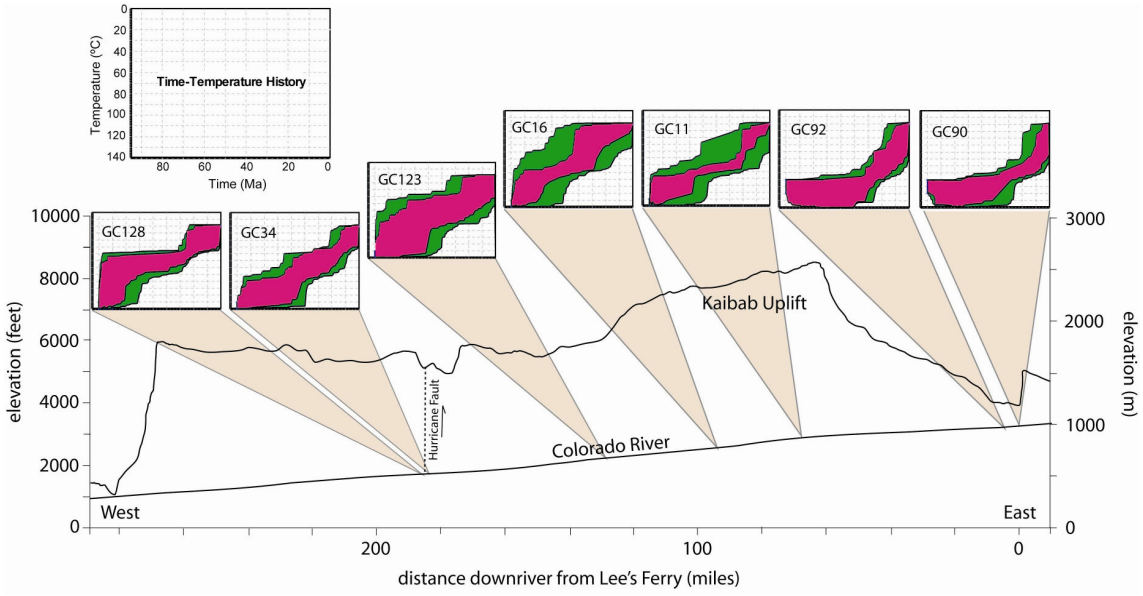
Time-Temperature History
Temperature (°C)
Time (Ma)
GC128
GC34
GC123
GC16
GC11
GC92
GC90
Kaibab Uplift
Hurricane Fault
Colorado River
West
East
elevation (feet)
elevation (m)
distance downriver from Lee's Ferry (miles)

Figure 2.4. An Age/elevation plot showing all vertical transects (with the exception of the Saddle Horse Canyon data), including the Wate borehole data and apatite fission track data (from Dumitru et al., 1994).

Figure 2.5. An age/depth plot of apatite (U-Th)/He data from boreholes (core) on the Coconino Plateau. All borehole surfaces were drilled atop the Kaibab Limestone.

Age/Elevation Plot - Vertical Transects

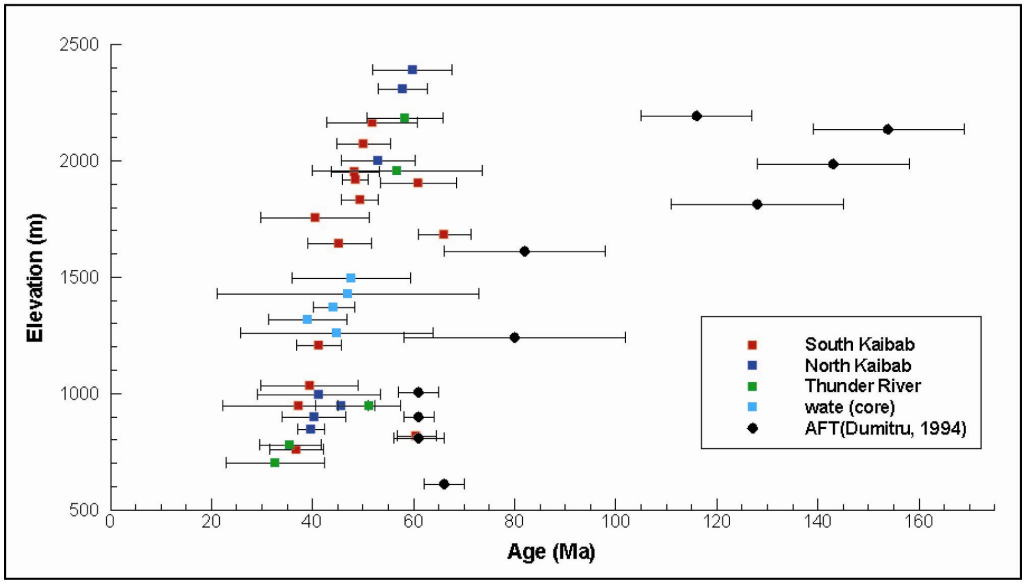

Age/Depth Data - Borehole Samples

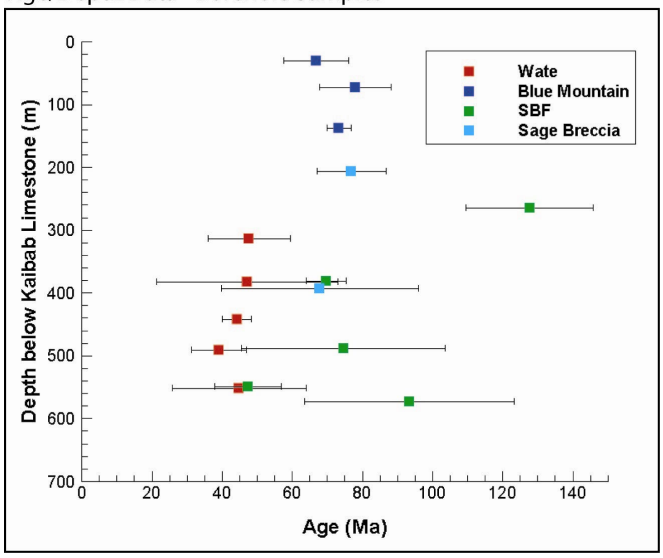

Figure 2.6. An age/topography profile of the Grand Canyon. A) Age distribution for fission track and (U-Th)/He data. B) The approximate topographic profile of the north rim of the Grand Canyon, and the surface profile of the Colorado River from Lee's Ferry to the Grand Wash Cliffs.

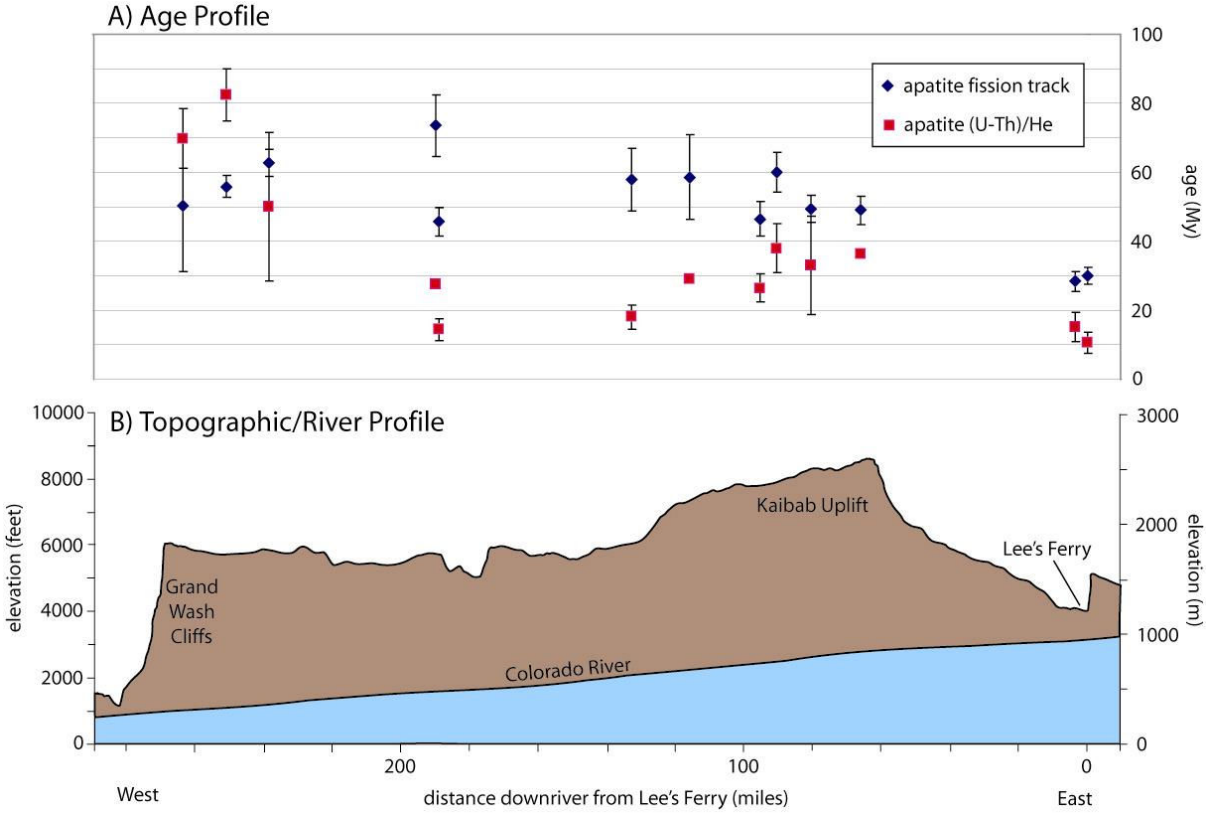
A) Age Profile
apatite fission track
apatite (U-Th)/He
age (My)
100
80
60
40
20
0
B) Topographic/River Profile
elevation (feet)
10000
8000
6000
4000
2000
0
3000
2000
1000
0
elevation (m)
Kaibab Uplift
Lee's Ferry
Grand
Wash
Cliffs
Colorado River
200
100
0
West
distance downriver from Lee's Ferry (miles)
East

Figure 2.7. An interpreted, time-stepped, unroofing profile for the Grand Canyon region based on overburden calculations generated in Table 2. Vertical red lines mark approximate calculated overburden thickness.

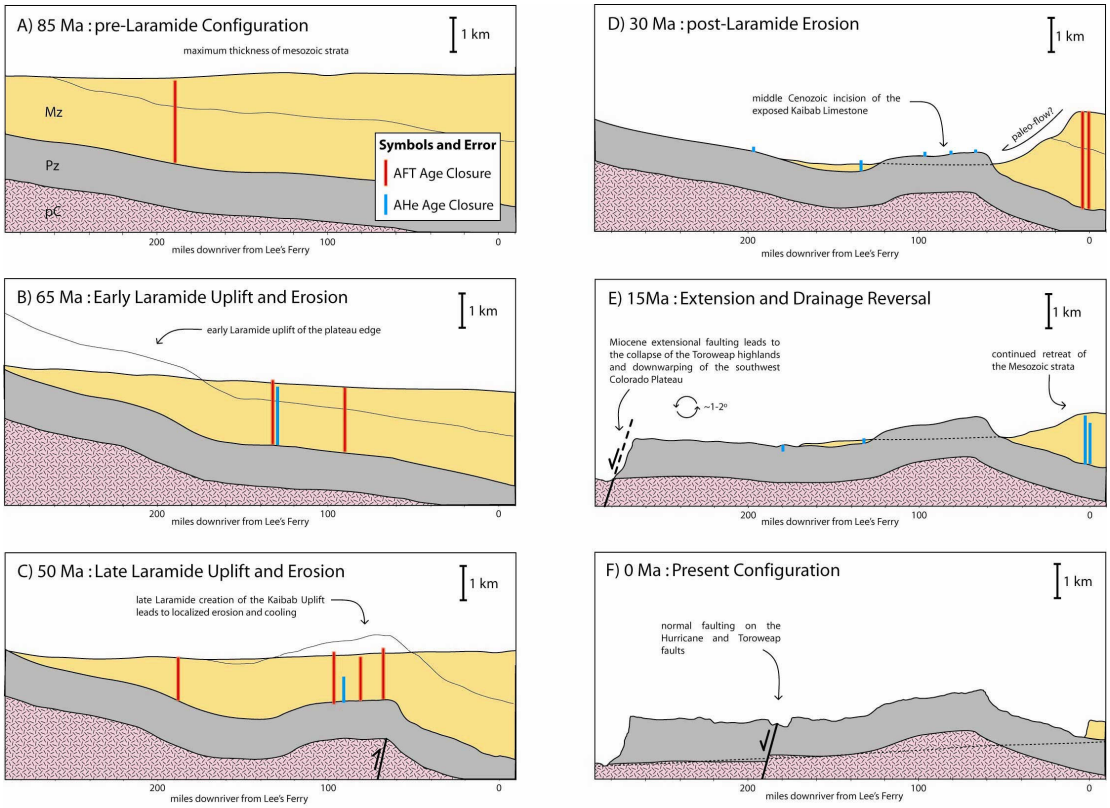
A) 85 Ma : pre-Laramide Configuration
maximum thickness of mesozoic strata
1 km
Mz
Pz
pC
Symbols and Error
AFT Age Closure
AHe Age Closure
200
100
0
miles downriver from Lee's Ferry
B) 65 Ma : Early Laramide Uplift and Erosion
1 km
early Laramide uplift of the plateau edge
200
100
0
miles downriver from Lee's Ferry
C) 50 Ma : Late Laramide Uplift and Erosion
1 km
late Laramide creation of the Kaibab Uplift
leads to localized erosion and cooling
200
100
0
miles downriver from Lee's Ferry
D) 30 Ma : post-Laramide Erosion
1 km
middle Cenozoic incision of the
exposed Kaibab Limestone
paleo-flow?
200
100
0
miles downriver from Lee's Ferry
E) 15Ma : Extension and Drainage Reversal
1 km
Miocene extensional faulting leads to
the collapse of the Toroweap highlands
and downwarping of the southwest
Colorado Plateau
~1-2°
continued retreat of
the Mesozoic strata
200
100
0
miles downriver from Lee's Ferry
F) 0 Ma : Present Configuration
1 km
normal faulting on the
Hurricane and Toroweap
faults
200
100
0
miles downriver from Lee's Ferry

Appendix A. Calculation of Thermophysical Parameters

Thermal Diffusivity and Volumetric Heat Production:

Thermal parameters for this study are meant to be roughly characteristic of the southwest Colorado Plateau, but intensive parameter characterization and sensitivity analysis will be pursued in upcoming investigations. Thermal diffusivity and volumetric heat production were largely calculated from typical lithologic parameters and applied to a crustal structure defined by geophysical and xenolithic data (i.e. (Condie and Selverstone, 1999)). A calculation spreadsheet was constructed to quantify a crustal average for thermal diffusivity and heat production. Relative lithologic proportions for each of the four crustal layers defined are used to calculate characteristic parameters for each of the four layers. Subsequently, these values are then weighted and averaged for the volumetric proportion of each of the four layers to calculate a total crustal average.

Table 3. Calculation of Thermal Diffusivity and Volumetric Heat Production

	Sed*	Upper*	Middle*	Lower*	Density (kg/m³)	Specific Heat (J/kg K)	T. Conductivity (W/m K)	T. Diffusivity km^2/myr
Lithologic proportions								
Sandstone	0.35				2500	964[1]	2.6[2]	*34.0*
Shale	0.45				2500	800	2.6[2]	*41.0*
Limestone	0.2				2500	860[1]	2.6[2]	*38.2*
Mafic Volcanic		0.23			2900	788[1]	1.9[1]	*26.2*
Felsic Volcanic		0.13			2700	880	1.7[1]	*22.6*
Graywacke		0.33			2700	800	2.4[1]	*35.1*
Granite		0.31	0.15		2700	880[1]	3[3]	*39.8*
Tonalite			0.7	0.25	2800	880[1]	2.65[3]	*33.9*
Amphibolite			0.1	0.3	3000	775	2.46[3]	*33.4*
Garnet amphibolite			0.05	0.15	3100	775	2.46[3]	*32.3*
Pyroxene granulite				0.1	3000	775	2.6[3]	*35.3*
garnet granulite				0.2	3100	775	2.6[3]	*34.2*
TOTAL	1	1	1	1				
A(uW m³)*	1.99	1.23	1.10	0.54				
Density(average)	*2500*	*2746.0*	*2820.0*	*2985.0*				
Specific Heat(average)	*869*	*832*	*864*	*801*				
Thermal Conductivity	*2.6*	*2.4*	*2.7*	*2.5*				
Thermal Diffusivity	*38*	*33*	*35*	*34*				

	Thickness (km)	Q (mW*m²)	A (°C/my)	Density (kg/m³)	Specific Heat	Thermal Conductivity	Thermal Diffusivity	Weighing Factor
Sedimentary	2	4	0.09	116.3	40	0.12	1.77	0.05
Upper	10	12.3	0.29	638.6	194	0.55	7.65	0.23
Middle	15	16.5	0.38	983.7	301	0.93	12.10	0.35
Lower	16	8.6	0.20	1110.7	298	0.95	12.54	0.37
Qc (four layers)	43	41.3						
Qm (= Qo - Qc)		20.7						
Qo observed		65						
Total Average			***0.96***	***2849.3***	***834***	***2.6***	***34.1***	

* Condie and Selverstone, 1994

[1] Ehlers, 2005

[2] calculated from SMU geothermal database averages

[3] Chapman, 1986

calculated values

Appendix A. continued…

Base Temperature

Base temperature and model thickness largely define the geothermal gradients modeled in Pecube. Therefore , particular attention was paid to the calculation of a base temperature. Existing matlab routines (Ehlers et al., 2005) were used as a base for these calculations. Input parameters were adjusted to values listed in Table 4 to create geothermal gradients characteristic of the southwest Colorado Plateau.

Table 4. Matlab Parameters for Calculation of Geothermal Gradient and Base Temperature

Parameter	Value	Units
Thermophysical Parameters		
Thermal Conductivity	3.0	(Wm/k)
Surface Heat Flow	0.065	(Wm^2)
Surface temperature	0	(ºC)
Depth to Lower Crust	2700	(m)
Depth to Upper Mantel	4300	(m)
Surface heat production	2.08E-05	(Wm^3)
Heat production for lower crust	5.40E-07	(uWm^3)
Heat production for upper mantel	2.00E-08	(uWm^3)

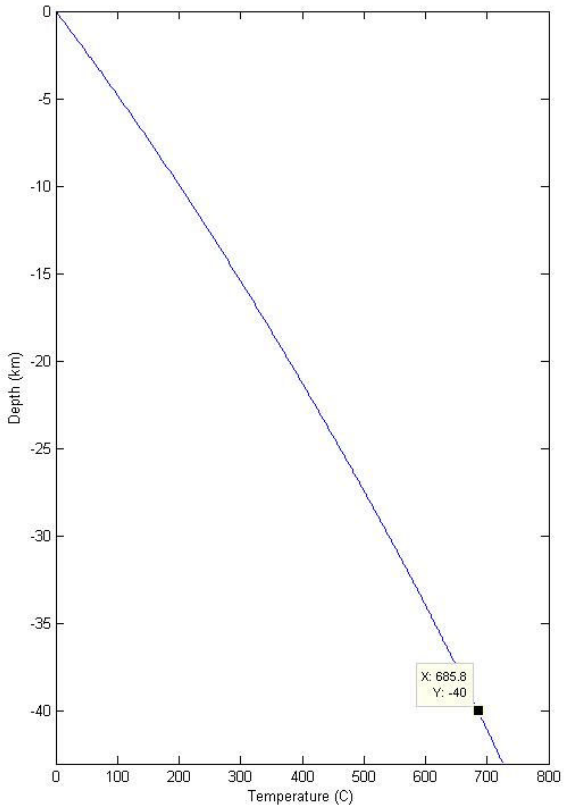

Appendix B. Grainsize/Age Correlation Test

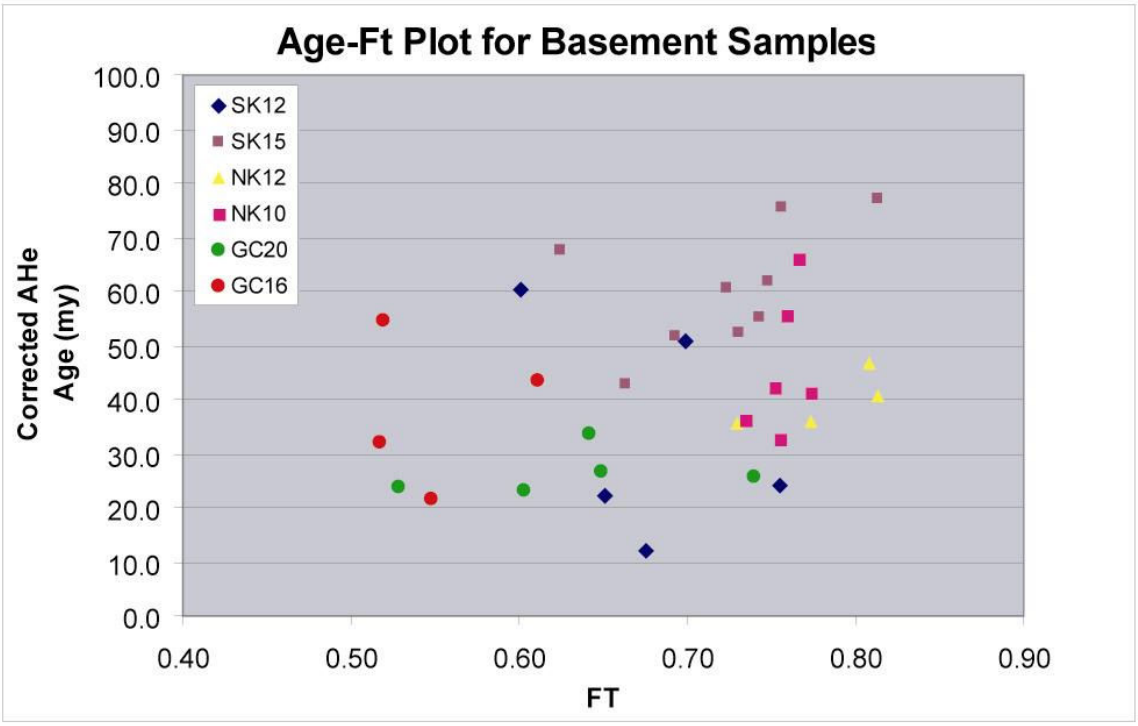

Appendix C : Overburden Calculations

Constants

	value	+-
Surface Temperature (ºC)	10	0
Thermal Gradient (C/km)	25	1
apatite (U-Th)/He closure (ºC)	50	2
apatite FT closure (ºC)	90	2.5

Ts - Avg. Surface Temp(ºC)
Ts - Sample Temp(ºC)
Es - Sample Elev(m)
Ek - Kaibab Elev(m)
Eu - pЄ/Pz Elev(m)
KND - Kaibab Normalized Depth(m)
OBt - Total Overburden(m)
OBmz - Mesozoic Overburden(m)

			Observed Parameters						Calculated Parameters				
River Mile	Sample(s)	age type	Age	+-	Es	Ek*	Ts	+-	KND	OBt	+-	OBmz	+-
191	01GC-128	AFT	74	9	485	2100	90	2	1615	3200	417	1585	417
191	01GC-128	(U-Th)/He	28	1	485	2100	50	2	1615	1600	288	-15	288
190	98GC-34	AFT	46	4	488	2280	90	2	1792	3200	417	1408	417
190	98GC-34	(U-Th)/He	14	3	488	2280	50	2	1792	1600	288	-192	288
134	02GC-123	AFT	58	9	610	2040	90	2	1430	3200	417	1770	417
134	02GC-123	(U-Th)/He	18	9	610	2040	50	2	1430	1600	288	170	288
96	98GC-20	AFT	47	4	720	2100	90	2	1380	3200	417	1820	417
96	98GC-20	(U-Th)/He	27	5	720	2100	50	2	1380	1600	288	220	288
91	98GC-16	AFT	60	6	731	2230	90	2	1499	3200	417	1701	417
91	98GC-16	(U-Th)/He	38	14	731	2230	50	2	1499	1600	288	101	288
81	98GC-11	AFT	49	4	768	2340	90	2	1572	3200	417	1628	417
81	98GC-11	(U-Th)/He	33	8	768	2340	50	2	1572	1600	288	28	288
67	01GC-103	AFT	49	4	841	2110	90	2	1269	3200	417	1931	417
67	01GC-103	(U-Th)/He	36	6	841	2110	50	2	1269	1600	288	331	288
4	01GC-92	AFT	28	3	951	1100	90	2	149	3200	417	3051	417
4	01GC-92	(U-Th)/He	15	9	951	1100	50	2	149	1600	288	1451	288
0	01GC-90	AFT	30	2	951	1100	90	2	149	3200	417	3051	417
0	01GC-90	(U-Th)/He	11	6	951	1100	50	2	149	1600	288	1451	288

Ek* - values are calculated from a linear extrapolation line extending from the South Rim to the North Rim over the sample location - see appendix B

Table 3. Overburden calculation spreadsheet

Appendix D : Kaibab Surface Projections

In order to calculate Kaibab normalized depths (KNDs), each sample must have to elevation of the Kaibab erosion surface directly above the sample. Because most samples were collected inside the Grand Canyon, most samples do not have the Kaibab limestone directly overhead. Because the Kaibab surface is non-horizontal, projections across canyon, over the sample of interest, are created to allow a the calculation of the projected (i.e. restored) Kaibab elevation. Each profile below shows the topographic surface along with a projected Kiabab surface across the canyon, and a vertical and horizontal projection of the sample location.

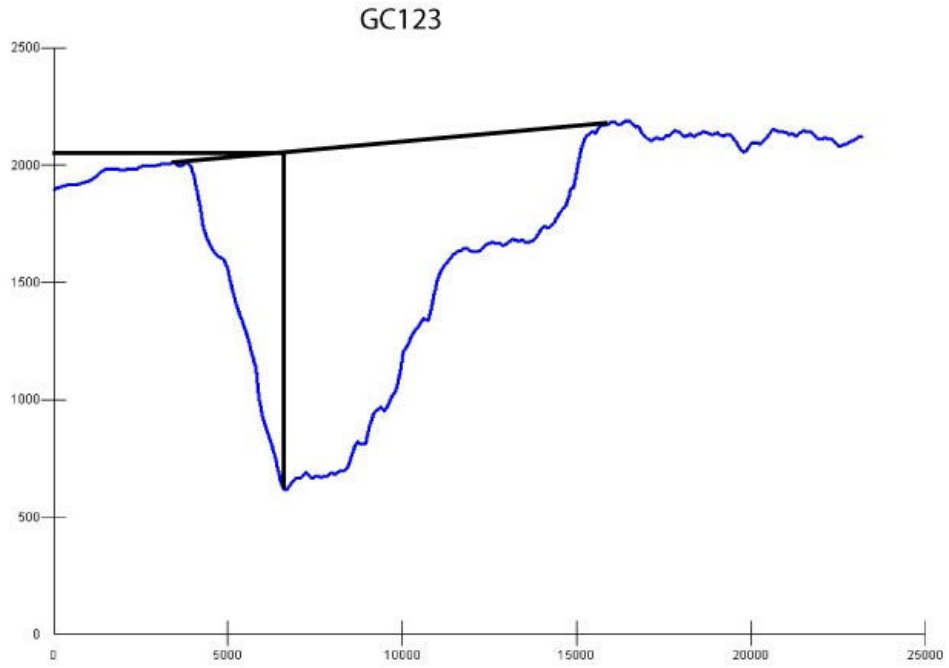

98GC20

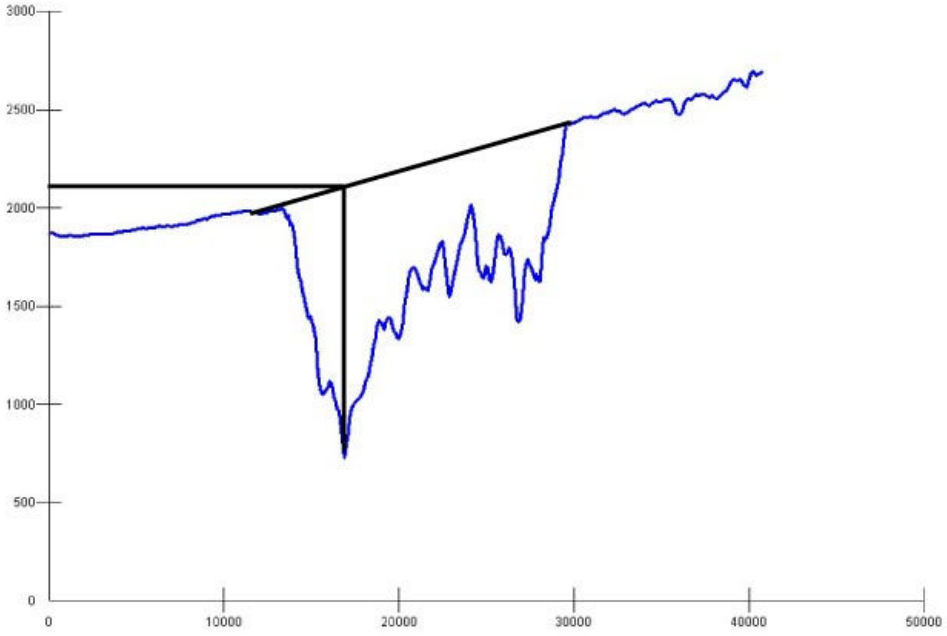

98GC16

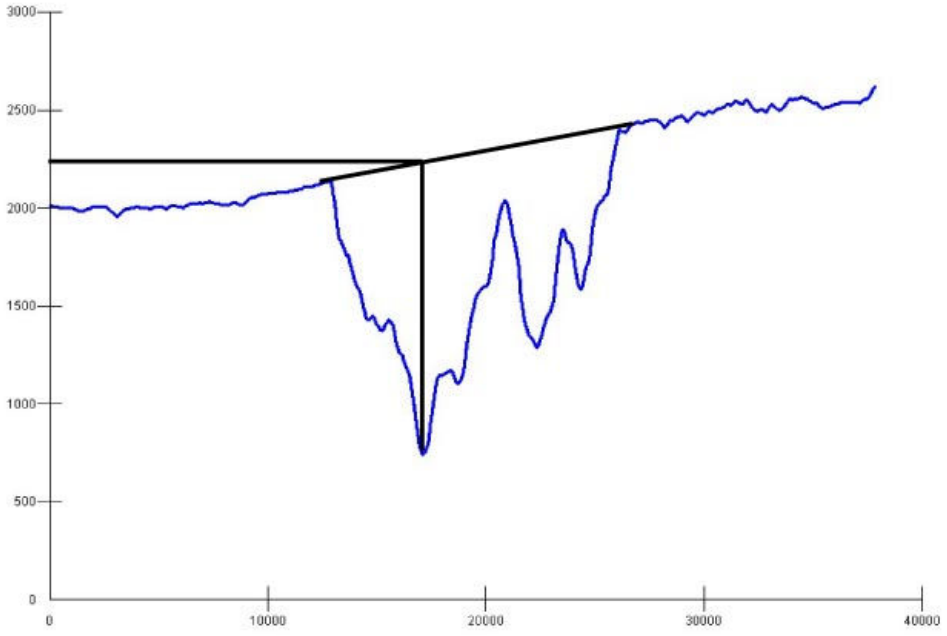

98GC11

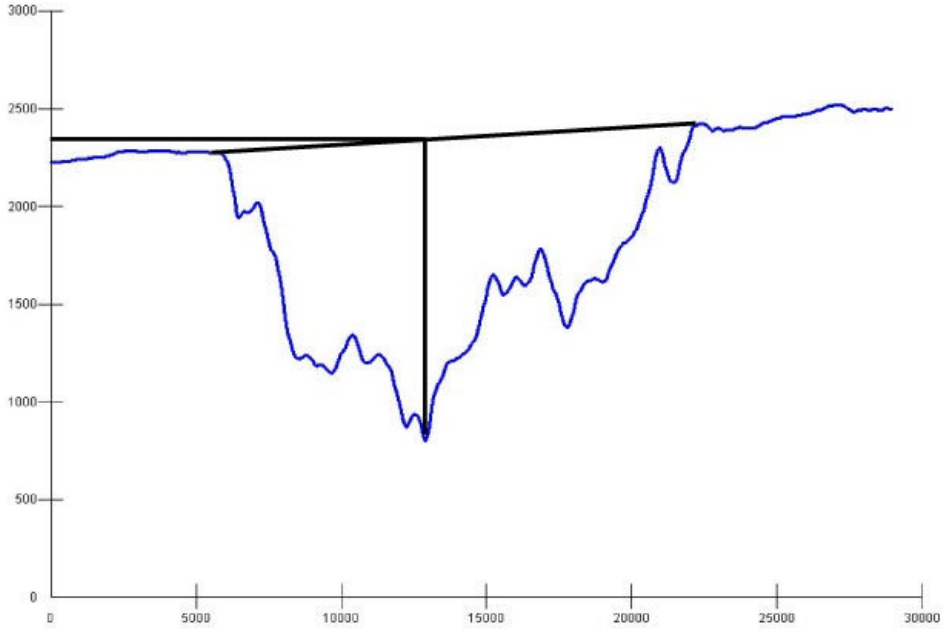

01GC-103

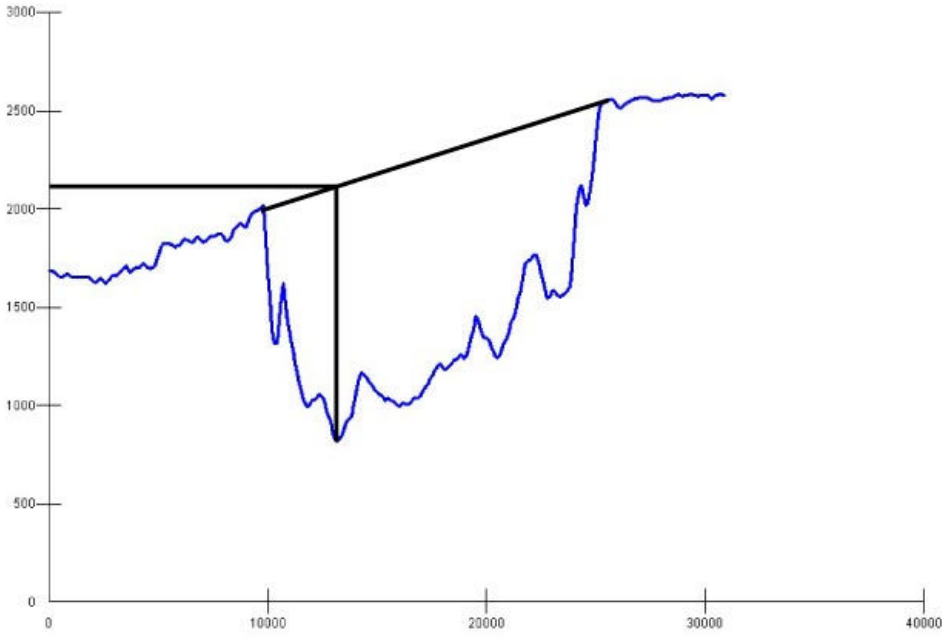

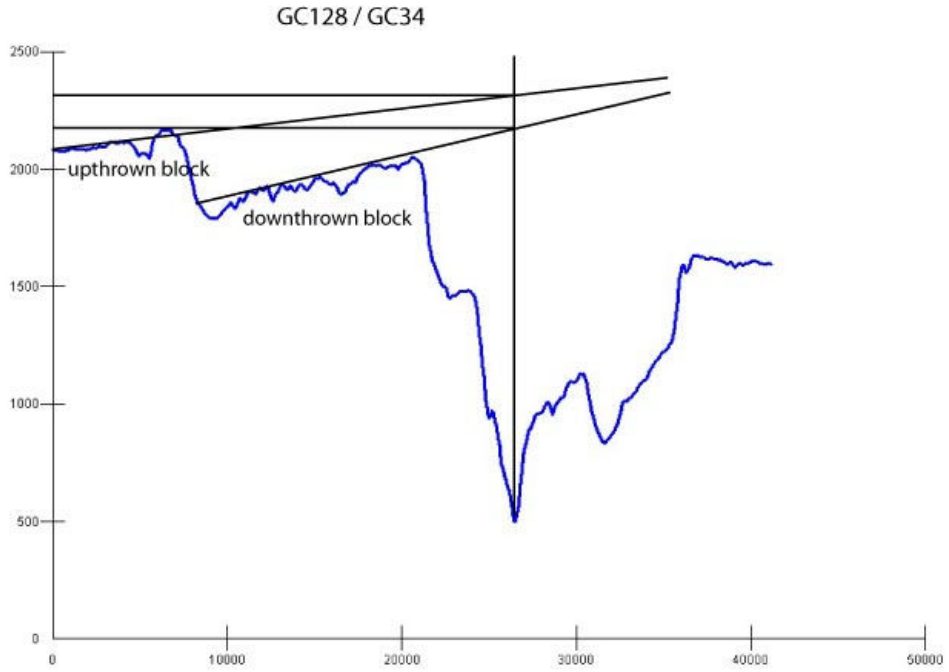
GC128 / GC34
2500
2000
1500
1000
500
0
upthrown block
downthrown block
0
10000
20000
30000
40000
50000